THE ADVANCED MANIPULATION OF AN ELECTROSPRAYED DIELECTRIC FLUID USING ELECTRIC FIELDS

by

Robert Logan Garris

A thesis submitted to the faculty of
The University of North Carolina at Charlotte
in partial fulfillment of the requirements
for the degree of Master of Science in
Applied Energy and Electromechanical Systems

Charlotte

2016

Approved by:

_____
Dr. Maciej A. Noras

_____
Dr. Mesbah Uddin

_____
Dr. Wesley Williams

ABSTRACT

ROBERT LOGAN GARRIS. The advanced manipulation of an electrosprayed dielectric fluid using electric fields (Under the direction of DR. MACIEJ A. NORAS)

The objective of this research is to investigate the control of sprayed gasoline using electric fields. This research was separated into three main parts including: charge repeatability, charge magnitude, and control of a sprayed injection. Using the triboelectric charging method, the dielectric was passed through two different materials and the net charge was measured. The gasoline (dielectric liquid) was sprayed into a chamber where the spray plume is observed for change in diameter with and without an electric potential applied. Four different injection pressures 103, 138, 172, and 207 kPa (15, 20, 25, 30 PSI) were used to test the charging capability of the dielectric while the injection time was kept constant. Charging results showed that the fluid could be charged at a maximum of -0.259 nC/g using the tribocharging method. The tubing section for the specified materials was lengthened to increase overall net charge. By increasing the pipe length one foot, the net charge increased. However, the magnitude increase of the overall net charge was not significant. Theoretically, if the pipe was continued to be lengthened the injection charge would increase.

Entrainment of the injected profile for the charged fuel was investigated for four different test injections at 138 Kpa (20 PSI). The event was captured using a high speed camera that accrued optical data at 1000 frames per second (FPS) at a vertical observation angle. Two different testing environments with and without electric potentials applied to the injection chamber were investigated. The testing layout is as follows: Injection 1 – no electric potential applied, Injection 2 – electric potential applied

10000 V, Injection 3 – no electric potential applied, Injection 4 – electric potential applied 10000 V. Comparison was achieved by taking x and y measurements at different frame intervals during injection. Compression of the injection event was achieved over the charged section of the chamber. For injections 1 and 2, maximum displacement was found to be 1.7 mm radially for the x direction and 3.7 mm in the y direction. Maximum displacement of the comparison of injection 3 and 4 in the x and y direction was 0.9 mm and 2.0 mm respectively. All testing was completed at atmospheric pressure 101325 Pa and at room temperature 297K.

ACKNOWLEDGMENTS

I would like to personally thank the college of Engineering Technology for all their support and for allowing me to use their resources. I would also like to thank the department for their generous funding that has allowed me to buy initial equipment needed to build my test setup. I would like to personally thank my adviser, Dr. Maciej A. Noras, for his persistence and encouraging technical advice throughout the duration of this project. I have been able to utilize his broad spectrum of knowledge to guide and encourage me to investigate new technologies as well as getting me excited about this research area. He is such a wonderful resource for all UNCC students and has helped countless amounts of people achieve their goals. I would also like to thank my committee members, Dr. Wesley Williams and Dr. Mesbah Uddin for their constant support and expertise. Without the ability to 3D print parts under Dr. Williams's guidance, I would not have been able to timely produce parts and make modifications to my design for testing.

I would like to give special thanks to Dr. Peter Tkacik and the engineering motorsports department for allowing us to use their high speed camera to capture results. Without his practical knowledge and resources this project would not have been possible. His help in operating and setting up our test unit was very beneficial to the completion and advancement of this research.

I also would like to thank my classmate Brett Cockerham for his help with programming the controller used for injection and for allowing me to vent when needed. Lastly, I would like to thank Alzarrio Rolle for his help in all areas of this research and for encouraging me to complete and further my investigation.

Finally, many thanks to the University of North Carolina at Charlotte Graduate School for allowing me to continue my education and for all the great experiences that I have gained while attending school. Thanks to my family and friends who have supported me throughout my education.

TABLE OF CONTENTS

CHAPTER 1: INTRODUCTION

Today's internal combustion engines are continually enhanced with the advancement of the injection and combustion processes to improve operating factors including: power output, emissions, fuel economy, and overall efficiency. High pressure common rail fuel injection systems and advanced nozzles have been implemented to optimize engine performance. These advancements improve control over the injection process, significantly increasing injection pressure and manipulating the duration of spray [1]. Injection pressure has a defined effect on the fuel during the injection process by increasing the droplet penetration depth and decreasing the fuel droplet size. This results in refining of the combustion process by enhancing the fuel-air mixture and maximizing atomization of the fuel droplets [2]. With advanced research in the injection to combustion processes, a more complete burn is achieved thus decreasing emissions and increasing fuel economy.

The internal combustion engine operates based on a four stroke cycle: intake, compression, power, and exhausts. Diesel oil and Gasoline are the two major fuel types that are used in IC engines. Gasoline engines operate at lower temperatures and pressures than diesel engines and produce fewer emissions. The operating efficiency of a gasoline engine is currently low at 36%. This has led to an increase in interest for research involving the IC engine, including the exploration of advanced spraying methods.

Electrospraying is a century old technique [3] that has been vastly utilized in many fields of science and technology. One of the unique applications for which it has also been considered is atomization and dispersion of fuel for advanced injection methods [4]. When the fuel droplets are small and well mixed with air, the combustion process is cleaner and more complete [5, 6]. In gasoline and diesel engines, depending upon the type of injector features, the droplet saunter mean diameter (SMD), defined as the diameter of the droplet with the same surface to volume ratio as that of the overall spray, is in the range of 120–200 μm [7]. Electrospraying can change the SMD to a much finer range. Values ranging as low as 10 μm have been reported [8, 9]. The process works well in atmospheric pressures [10]. Achieving appropriate atomization and fuel to air ratio is just an initial step into the injection process. Typical pressures in a cylinder of a car reach up to 20 MPa (Diesel engines) and that prevents the fuel from dispersing properly within the engine's cylinder. In order to entrain the fuel further into the cylinder volume, very high injection pressures are used.

First implementation of electrospraying in a working car engine was demonstrated by Anderson [11], but the gains in engine performance and reduction in emissions were relatively small. The electrosprayed droplets were not penetrating the cylinder depth sufficiently, and had a tendency to drift toward the grounded walls. The resulting recommendations were to increase the fuel charging and introduce appropriate control techniques. No specific methods were proposed, however in the earlier work by Shrimpton [4] a suggestion was made to attempt controlling the plume of electrosprayed fuel by use of electric AC or DC fields, however no practical implementation of that idea was provided. This work presents an attempt on control of electrosprayed fuel using

external electric fields in an engine cylinder-like geometry.

The purpose of this study is to entrain the injected profile of charged gasoline by applying an electric potential to an atmospheric chamber for purpose of possible improvements to engine efficiency and emission reductions with a proven concept. Three main parts will be studied: fuel charging, fuel injection/dispersion, and atomized fuel control within an electric field chamber. To test the charging capability of the fuel, repeatability of charging based on different injection pressures and the triboelectric charging method using teflon and nylon will be investigated. The net charge applied to the sprayed fluid will be evaluated using a Faraday cup. A test spray chamber will be built to control the movement of electro-sprayed fuel at atmospheric pressure to investigate the concept for controlling the spray pattern of the specific dielectric fluid. The directional control component will be investigated by applying an electric field to manipulate the forces seen on the spray pattern. A simulation model has been created in COMSOL Multiphysics and will be implemented to validate accuracy based on test parameters. This research will lay the ground work for furthering the investigation into advance implementation of controlled electro-sprayed fuel in high pressure environments.

CHAPTER 2: LITERATURE REVIEW

2.1 Injection Process – Overview

There are two types of injection methods for IC engines. Port fuel injection (PFI) and gasoline direct injection (GDI). PFI is the process of injecting fuel into a mixing chamber outside of the engine cylinder allowing the fuel and air to mix prior to the injection stroke of the engine. GDI is the process of directly injecting the fuel into the engine cylinder. The GDI method has been developed in the last decade to improve control over the injection process. Figure 1 below shows how the injector has moved in comparison to the PFI engine[7].

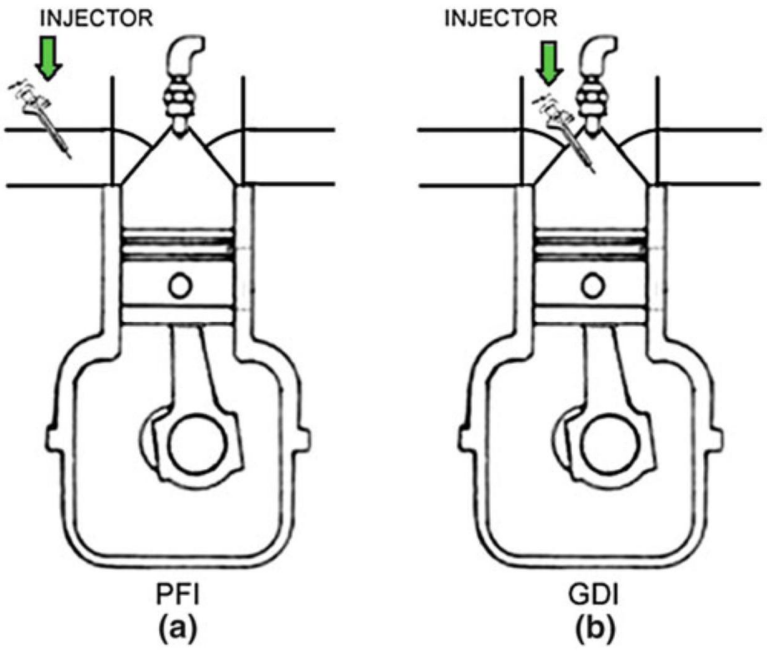

Figure 1: GDI (a) vs PFI (b) injector placement [7]

The PFI system does not include the ability to change how the system is controlled when injected into the cylinder. The fuel air mixture is pulled into the chamber leaving little room for modification to the physical injection process. The operating advantages that can be seen from using a GDI system include higher engine efficiency and a reduction in fuel consumption. The GDI allows for increased control over the injection of the fuel while maintaining lower pump losses [7]. The disadvantage of the GDI system is the increase in particulate matter and NO_x resulting in a need for additional hardware to trap these emissions [7]. Control of the injection process and the overall operation of the engine are done by the Electronic Control Unit (ECU). It collects all data recorded by sensors and commands actuators for efficient and smooth operation [7].

Newer engines operating with GDI use high pressure common rail fuel injection systems (CRI) and highly modified injection nozzles. The CRI system has been implemented to minimize the negative effects seen from the GDI method such as increased emissions. The CRI systems can decrease the duration of the injection time and also include pre-spraying at different periods in the compression cycle. CRIs supply fuel to each electro-injector at a high pressure using a common rail as seen in the Figure 2 below.

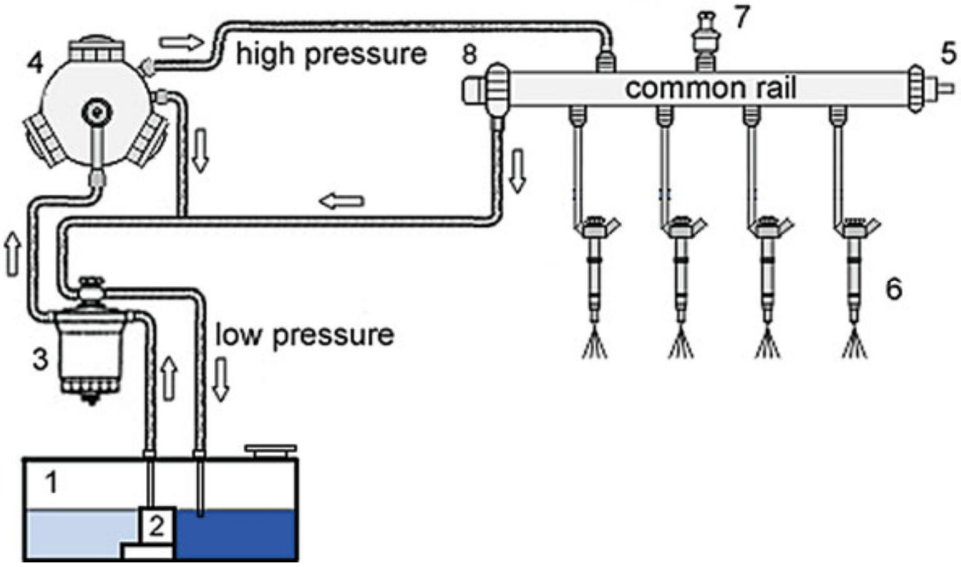

Figure 2: CRI System (1-tank, 2-fuel pump, 3-filter, 4-high pressure pump, 5-manifold, 6-injectors, 7-pressure sensors, 8-pressure regulation valve) [7]

After injection using a CRI system the fuel profile begins to break apart into smaller droplets. Researchers have observed the breakup periods to determine how individual droplets affect one another. Different breakup periods have been considered to fully understand how the atomizing droplets change during injection to better understand how the fuel-air mixture can be optimized [12]. There are two known atomization processes during standard injection: primary and secondary atomization [12]. Primary atomization occurs close to the injection nozzle and is the first breakup sequence [12]. The fuel jet separates into large and small liquid droplets as seen in Figure 3.

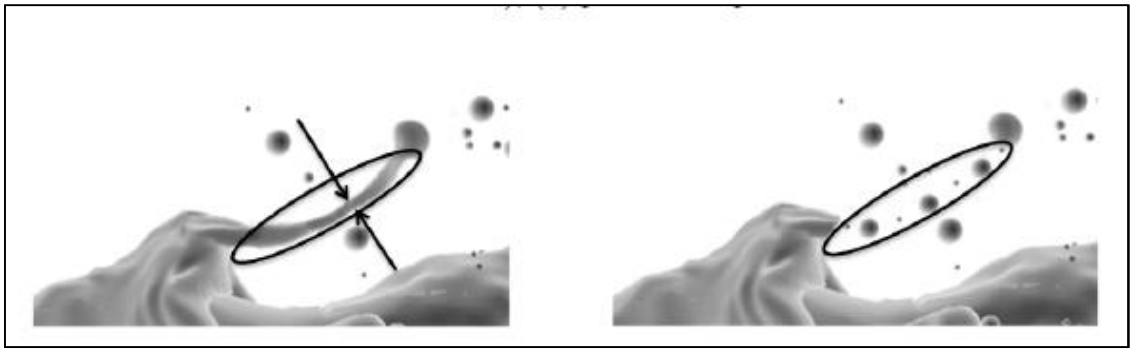

Figure 3: Breakup of fluid into spherical droplets [12]

Secondary atomization is the further breakup of the fuel deeper in the cylinder producing smaller droplets [12]. Other complex reactions from the high pressure nozzles include cavitation at the orifice and evaporation of the fuel in the cylinder due to the high pressures and temperatures during engine operation[12]. Key characteristics that can be defined during the injection process that affect the operation of an IC engine are the STP and CSA. STP or Spray Tip Penetration is the furthest distance from the nozzle tip to the spray limit [13]. The CSA or cone spray angle is the angle between the different spray directional lines of fuel [13]. Refer to Figure 4 for an illustration of the STP and CSA of an injection profile.

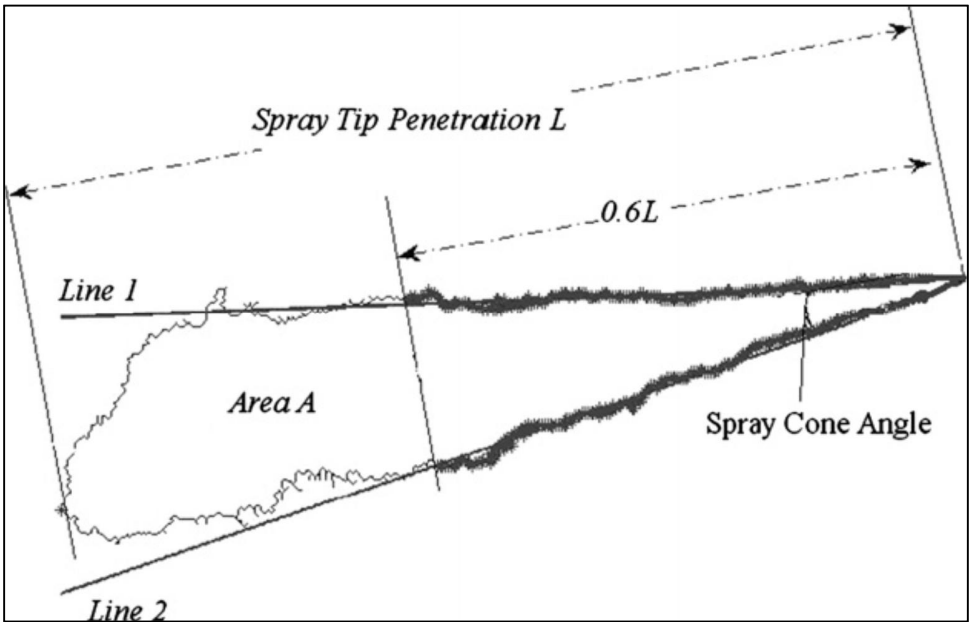

Figure 4: Definition of spray characteristics [13]

Highly-dispersing nozzles decrease the injection duration allowing more time for the fuel and air to mix improving the amount of fuel combusted. This is in part due to the short injection time when operating at a high injection pressures. Improving the overall burn inside of the combustion chamber decreases emissions that are created during the power stroke. Flatter spray patterns or increasing the cone spray angle can also be

beneficial in producing less emission, increasing spray area, and decreasing the potential for the wet wall effect [13]. The wet wall effect is the point at which fuel reaches the wall of the cylinder increasing the amount of fuel that is not fully combusted.

2.2 Combustion Process

The output performance of an Internal Combustion Engine depends on the quality and completeness of the burning process. Combustion inside of the cylinder occurs when the ignition temperatures are reached or a spark plug ignites the fuel [14]. The extreme increase in temperature occurs due to the compression of gases by the piston and allows the fuel to be above the flammable threshold [15]**.** This step in the combustion cycle is known as the compression stroke.

Most engines today operate using either diesel fuel or gasoline as the burning fluid. These fuels make up 98% of the energy used in transportation today [16]. The main differences between the fuels are the way the burning process is initiated and the operating characteristics of the engines. Diesel fuel does not require a spark to ignite. The fuel relies on the temperature inside the cylinder reaching a threshold value that will ignite the fuel-air mixture. This results in engines that operate under higher temperatures and pressures. However, both engine type's operator using similar basic principles.

When analyzing the combustion efficiency of either type of engine, it can be observed that the CSA, STP, droplet velocity, and droplet size affect the point of atomization and can affect the ratio of the air-fuel mixture [13]. Higher air-fuel mixtures allow for a complete combustion and cleaner emissions due to decreased amount of particulate matter [1]**.** In the past efficiency of an engine has been increased by raising the compression ratio [14]. However, in this way negative effects can be introduced such as

knocking. Knocking is created when the combustion process speed is increased [14]. When using a high pressure injector, the STP is limited by the droplet size [11]. Max injection pressure can rise as high as 1800 bar or 180 MPa, and normal injection periods last from 0.5 ms to 1.5 ms [2]. The injection duration depends on the rail pressure and the quantity of the fuel. It is correlated that fuel consumption improves as injection pressure is increased.

With extreme fuel injection pressures (FIP) the fuel droplet size is reduced [17]. Atomization is improved significantly but STP is decreased. This can cause knocking and amplified engine noise. The CRI system allows for a very short injection duration which increases the amount of time the air-fuel mixture has in the cylinder before combustion. Other factors that affect the STP and CSA are the amounts of back pressure that is present in the cylinder [13]. Back pressure is created by the piston when it is in the compression cycle. When back pressure is amplified the STP is decreased. This causes opposite forces to act against the spray of the fuel limiting its penetration depth [13]. The CSA will increase which can cause the wet wall effect [17-19].

2.3 Electrospray Technology

Liquids can either be conducting or non-conducting. Conducting liquids have a lower electrical resistivity increasing the ability to charge the fluid. A material or liquid is considered to be a conductor if its conductivity is greater than 10^{-12} /Ωm. Non-conducting or insulating liquids have high electrical resistivity typical around 10^{10} Ωm. This work will focus on gasoline which is considered an insulating liquid due to its charging characteristics. Gasoline is also known as a dielectric fluid. A dielectric has charged

monopoles and dipoles that are equal but opposite and are separated by neutral entities [20].

During the 20th century electrospraying technologies were implemented into different sections of industry. The results from charging conducting liquids include producing coating uniformity, control targeting, and minimized power consumption and are found in applications such as; fine powder production, painting, microencapsulation, precipitation of pollutants, ink-jet printing, agriculture, and powder coating [20, 21]. Electrospraying is used when there is a desire to generate a fine mist by charging the fluid. Liquid is expelled through a nozzle-like device into a chamber or a designated location. When the liquid leaves the nozzle, it is immediately exposed to a high voltage electric field which results in producing small droplets. With the droplets in the working fluid now charged, this allows for a better and more even distribution of spaces between droplets, producing less coagulation. The benefits of electrospraying can be used in numerous applications such as surface coating, the production of thin-films and in electro scrubbing. Production of thin films can occur at micro or even nano magnitudes. The evolution of electrospraying has lead researchers to experiment with thinner films and the uses of substances such as fine powders [22].

Electrospraying is also being used in many other disciplines in science including microelectronics, modern material technologies and is most noted in medical research. Nano engineering of stem cells in medical science frequently interact with this process. The fluid from the nozzle travels a certain distance before it is electrically charged. At which point, the trajectory of the fluid becomes more complicated as it experiences more instabilities and other forces such as gravity and drag forces [23]. Droplets produced by

electrospraying can range from tens of nanometers to hundreds of micrometers in diameter. The profile can differ depending on the type of fluid, pressure, and temperature conditions [24].

Different innovative atomization applications have been tested including the use of electrospraying fuel. This physical system induces a charge on a dielectric fluid [20]. By inducing an electrical charge into the hydrocarbon fuel, uniform particle generation can be achieved [25]. This advanced method has been tested by charging using an electrode imbedded in an injection nozzle. Atomization injectors have been designed to apply a charge to dielectric liquids for the purpose of improving the overall charge applied to micro droplets [20].

The inquiry of electrospray has been investigated within the automotive industry to analyze the effects of charged fuel droplets as they are being sprayed. It is known that with electrostatic atomization, the breakup period of the fluid occurs sooner and results in smaller droplets [8]. The electrostatic force that acts on a fluid droplet can be explained using surface tension force vs electric field force. The desired charge can be applied using electric fields within the injection nozzle. When the dielectric fluid is induced, a surface charge is created leading to a significant decrease in time required for the fluid separation. This occurs when the total charge on the surface q, reaches a limited value called the Rayleigh limit and can be explained by the equation below.

$$q^2 = 8\pi^2\epsilon_0\gamma\frac{D^3}{2} \quad (1)$$

Where ϵ_o is permittivity of the medium surroundings, γ is the liquid surface tension, and D is the droplet diameter [8, 26]. Most of the results seen from electrostatic atomization have been observed at relatively low pressure and density environments. When the

electrospray process was observed under normal engine operation conditions, it was concluded that the charging of the fuel droplets at much higher injection pressure had less effect than at lower pressures. The particles were more difficult to charge because of a short contact time within the injector. Therefore, the advantages from creating a charge on the surface of the fuel droplets have a more significant effect in lower pressure applications [27, 28].

2.4 Triboelectric Charging

Triboelectric charging is the effect of utilizing friction to create an electric charge. The process of how the charging method works is not fully understood. One definition states that by rubbing two materials together one will lose electrons by physical contact [29]. The same effect can be seen when fluid is passed through a pipe. As the liquid flows a current creates a double layer, or two electrical zones, of opposite signs in the solid and the liquid [30]. Depending on the material properties this can be enhanced by the type of flow, laminar or turbulent, against the material[29]. There are two known regions created: the compact layer and the diffuse layer [30]. The compact layer is close to the wall and electrical charges are not affected by the fluid. The diffuse layer consists of a space charge density that decreases as it moves further from the wall [30]. The electrical double layer according to the Stem model can be represented Figure 5 below.

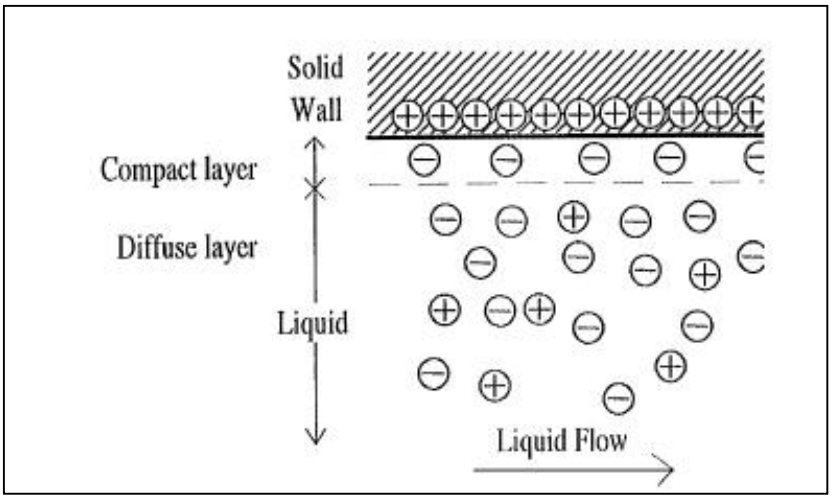

Figure 5: Stem model electrical double layer [30]

Therefore, the space charge reaches its maximum closest to the wall [30]. Other factors can affect the amount of charge applied including contact time, temperature, droplet size, and surface microstructure [31]. This method is attractive for charging fuel because it does not require a current source avoiding safety hazards. Teflon and nylon have both been proven to effectively charge powders for coating purposes [29]. The charge polarity depends on the material [32].

2.5 Proposed Technology

The purpose of the research is to evaluate a dielectric fluid gasoline for charging capability and repeatability using the triboelectric charging method to determine it can be controlled by electric fields at atmospheric pressure. An injection unit and electric field chamber was designed and built to test the above statement. This study will lay the ground work for furthering the investigation into improving how IC engine operate and to introduce an advanced spraying method with external control outside of the injection characteristics.

It is important to understand the basics of how the injection to combustion process is affect by conventional methods of injecting fuel at high pressures into the engine

cylinder. Therefore, when analyzing the injection to combustion process, it is evident that there are numerous factors involved in the atomization of fuel droplets within the cylinder before combustion. This is a dynamic system that is not easily modeled. Important parameters to consider when evaluating efficiency of an internal combustion engine process include aerodynamics of the inducted air, process and bounds of the injected fuel, and the specific design of the combustion chamber [19]. When manipulating the different analytical constraints such as cylinder pressure, injection pressure, and fluid density, the results seem to affectively improve one factor while impeding another. Therefore, this method of controlled injection will improve upon past injection methods to add an external control to optimize injection characteristics.

CHAPTER 3: METHODOLOGY

3.1 Mathematical Model

Pre calculations for the effect of applying an electric field to fuel particles have been evaluated using Stokes' Law for drag on a single particle for testing environmental conditions [33]. The ruling mechanical and electrical forces that were considered for this mathematical model include drag, gravitational, electric field, and space charge field. The driving equations are listed below:

$$F_{drag} = 6\pi\eta D_p u \tag{2}$$

Volume and mass of particle droplet:

$$V = \frac{4}{3}\,\pi\,\left[\frac{d_p}{2}\right]^3 \tag{3}$$

$$m_p = \rho\, V \tag{4}$$

Where d_p is the estimated diameter of the fuel particle, η is the viscosity of air at 297 K and at atmospheric pressure, du is the assumed velocity of the particle in the air that is considered to be nonmoving, and η is the air kinetic viscosity. The additional forces that were considered in this model were the gravitational force and also the electric force created from placing a charged particle inside an electric field.

$$F_{\text{gravity}} = g m_p \tag{5}$$

$$F\_el = qE \tag{6}$$

Where g is the gravity constant 9.81 [m/s^2], m_p is the particle mass computed using fuel density and assumed particle diameter, q is the approximated charge placed on a particle, and E is the electric field intensity evaluated at 0, 1, and 100 [kV/m]. Therefore the total force can be derived by using the below force balance:

$$m_p \frac{du}{dt} = \sum F(8)$$

$$m_p \frac{du}{dt} = F_{drag} + F_{gravity} + F_{el} \quad (7)$$

$$m_p \frac{du}{dt} = 6\pi\eta D_p u + g m_p + qE \quad (8)$$

Evaluating the forces that affect the motion of the particle toward the cylinder wall only considers the horizontal components that affect a single fuel droplet. This eliminates the force due to gravity which simplifies the equation to:

$$m_x \frac{du_x}{dt} = -6\pi\eta D_p u_x - qE_x \quad (9)$$

Assigned the constant value as $\tau = 6\pi\eta D_p$ (10)

$$m_p \frac{du_x}{dt} = -\tau u_x - qE_x \quad (11)$$

The solution provides the following equation

$$u_x = \frac{-qE_x}{\tau}\left(1 - e^{\frac{-t}{t_m}}\right) + u_{x0} e^{\frac{-t}{t_m}} \quad (12)$$

$$t_m = m_p/\tau \quad (13)$$

t_m represents the mechanical relaxation time. This value demonstrates how the particle will respond to the external forces applied by the electrical field. If the electrical forces that are applied to the medium are present for a short time in comparison to the relaxation time, the behavior of the fuel particle will be ruled by its inertia. Otherwise the particle will be controlled by the drag forces. Therefore the distance that is traveled horizontally toward the cylinder wall is:

$$x = \frac{-qE_x}{\tau}\left[t - t_m\left(1 - e^{\frac{-t}{t_m}}\right)\right] + u_{x0}t_m\left(1 - e^{\frac{-t}{t_m}}\right) + x_0 \quad (14)$$

Assume $x_0 = 0$ [m], initial position of the particle and $u_{x0} = 5$ [m/s], initial x direction velocity of the particle. The x direction velocity was calculated based on an injection angle of 30° (15° from the Vertical) at 20[m/s]. Initial calculations were done based on the fluid flow for the setup. This calculation estimates the injection velocity at 20 PSI ignoring losses due to piping geometry.

Table 1: Calculated velocity of injection

System Definition	Values	Units	Converted Values	Units	Description
Density Fluid	750	$\frac{kg}{m^3}$	750.00	$\frac{kg}{m^3}$	Fuel Density
Gravitational Constant	9.81	$\frac{m}{s^2}$	9.81	$\frac{m}{s^2}$	
Pressure 1	20	PSI	137.90	KPa	Pressure inside Tank
Pressure 2	0	PSI	0.00	KPa	Pressure at Nozzle Exit
Height 1	10	in	0.25	m	Height of Fluid inside Tank
Height 2	15	in	0.38	m	Height of Nozzle Exit
Velocity 1	0.00			$\frac{m}{s}$	Velocity of Fluid in Tank
Velocity 2 (Calculated)	19.11			$\frac{m}{S}$	Velocity at the exit of the Nozzle

3.2 Assumptions and Calculated Values

The values used for calculations were based on the testing parameters of the designed injection chamber environment. However, the fuel droplets were assumed to be charged to the maximum value based on the Rayleigh limit. Refer to the list below for value definitions.

$D_P = 50\ [\mu m] and\ 5\ [\mu m]$	Estimated fuel droplet size
$\eta = 18.47 \times 10^{-6}$ [Pa·s]	From Engineering Equation Solver built in heat transfer charts @ 297K
$\rho = 750\ \left[\frac{kg}{m^3}\right]$	Density of Fuel (Data from BP MSDS)
$\epsilon_0 = 8.85\ x\ 10^{-12}\ \left[\frac{F}{m}\right]$	Dielectric Permeability of Air
$\gamma = 2.58\ x\ 10^{-2}\ \left[\frac{N}{m}\right]$	Surface Tension of fuel @ 20 °C
$q_{electron} = 1.6\ x\ 10^{-19}\ [C]$	Charge of an Electron
$V = 6.55\ x\ 10^{-17}\ [m^3]$	Calculated volume - Equation (4)
$m_p = 4.90\ x\ 10^{-14}\ [kg]$	Calculated mass of a single particle - Equation (5)
$q = 1.50\ x\ 10^{-12}\ [C]$	Calculated charge based on Rayleigh limit - Equation (1)
$\tau = 2.27x\ 10^{-9}\ \left[\frac{kg}{s}\right]$	Calculated assigned Constant - Equation (12)
$t_m = 2.35\ x\ 10^{-5}\ [s]$	Mechanical relaxation time - Equation (15)

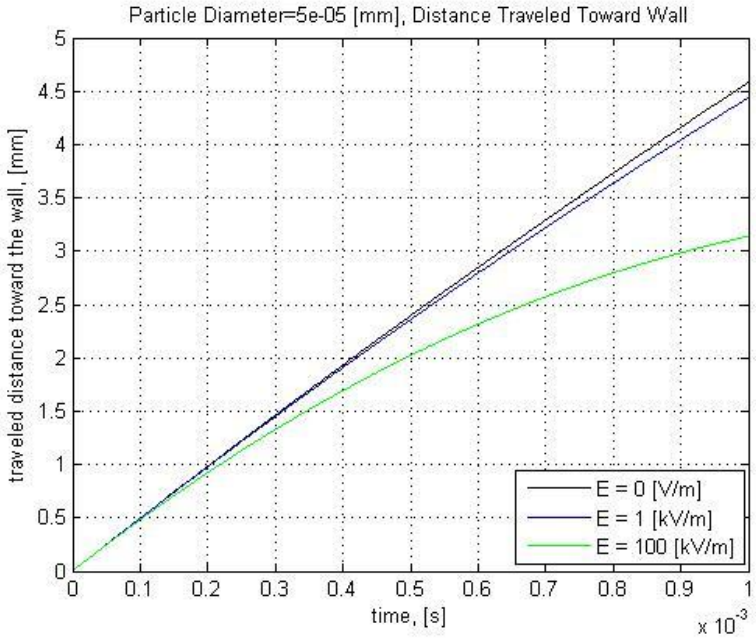

Figure 6: Distance traveled toward the wall at different electric field intensities

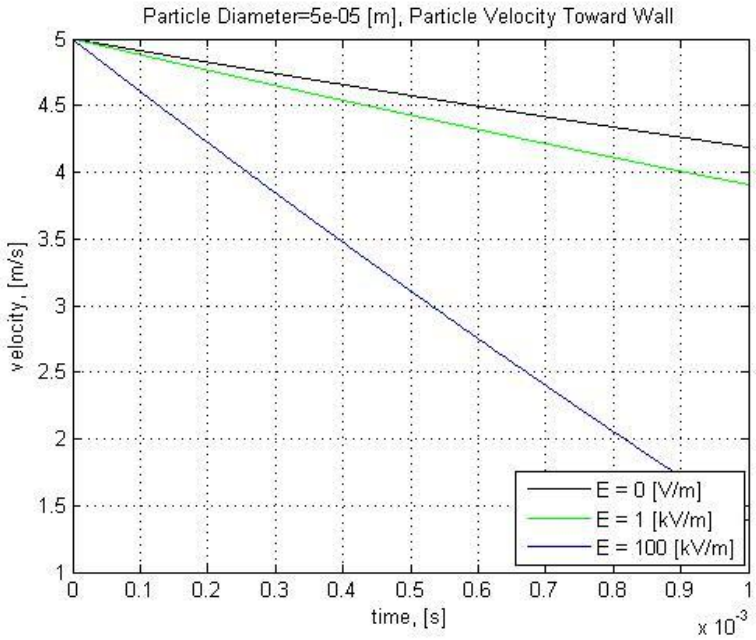

Figure 7: Particle velocity toward the wall for different electric field intensities

As shown in Figures 6 and 7, the fuel droplet trajectories toward the wall are controlled by the electric forces. The greatest difficulties associated with the control of micro-particles are applying an effective charge to the droplets. This places importance

on correctly designing the spray unit to apply an effective charge to the fuel jet during injection period. This model, evaluated for preliminary purposes does not consider the space charge influcence that is seen on the cloud of particles. The force is related to the distribution of the fuel droplets and does not affect all of the fuel particles equally. The droplets in the center of the cloud experience theoretically zero space electric forces, while the outside of the cloud is pushed toward the wall of the cylinder. The droplets in the center of the spray cloud are affected by all surrounding electric fields keeping them stationary. Smaller droplets were then evaluated using the same above condition with a diameter of 5μm.

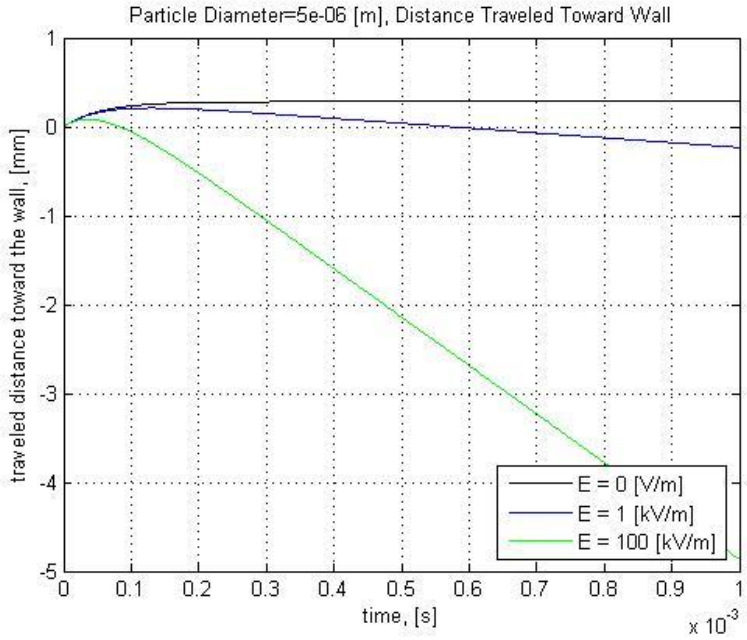

Figure 8: Distance traveled toward the wall at different electric field intensities for smaller diameter droplets

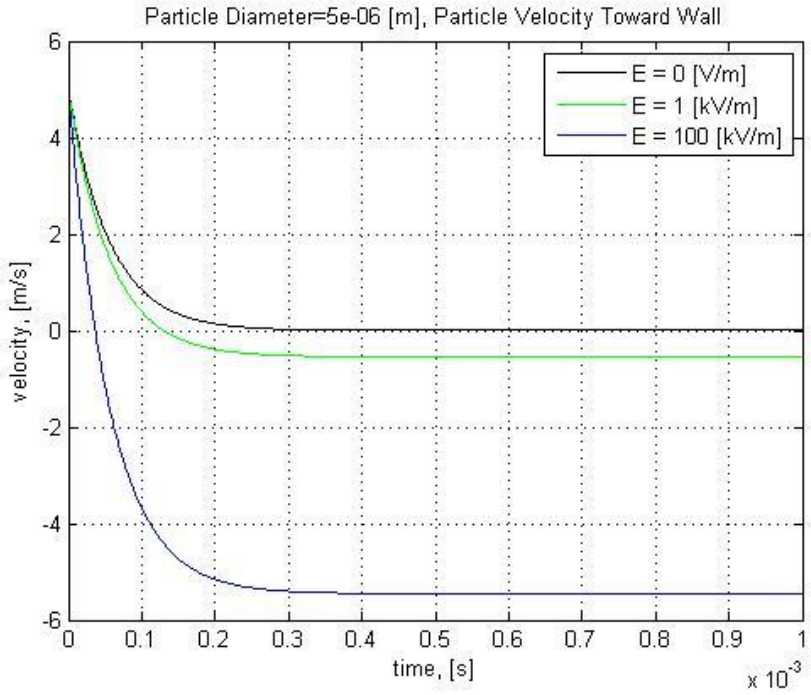

Figure 9: Particle Velocity toward the Wall for Different Electric Field Intensities for Smaller Diameter Droplets

Figures 8 and 9 above show the simulated results using a smaller droplet size. The effect is seen in the amount of movement in the negative direction away from the wall. The fuel droplets are controlled by the electrical force instead of being controlled more by their inertia due to the droplet size. This again considers a constant force electric field and does not demonstrate the affects seen on the droplets as they move farther away from the cylinder walls.

3.3 Research Definition and Test Parameters

Step 1 – Build testing spray unit

Step 2 - Test charging repeatability using Tribocharging method

Step 3 – Investigate directional control of charged injected fuel

To further this investigation, a test spray chamber and injection unit was designed and tested. This unit was used to investigate the theory discussed above to control charged fuel droplets. 87 octane gasoline was collected from a local gas station and tested for charging magnitude and repeatability of charge. Triboelectric charging was implemented as the source for inducing the charge in the fuel. A section of the piping was changed between teflon and nylon.

Controlling the direction movement of the injected fuel was attempted by creating an electric field to manipulate the fuel droplets. The field was created by applying a negative potential to the top section of the spray chamber repelling the negatively charged fuel droplets. The bottom section of the chamber was grounded. Initial estimation for operating nozzle injection pressure was in the range from 103 to 207 kPa. The pressure was generated by a diaphragm pump and was monitored by a pressure gage located in the flow path of the fuel. Initially a push valve was implemented to restrict the

flow and to release the injection processes. Modifications of the test chamber were completed to best optimize the chamber setup and to improve testing results.

3.4 Chamber Designs and Modifications

3.4.1. Injection Chamber Design

Mechanical Components:

- 3/8” Electrical Solenoid Valve 12 VDC
- Fuel Pressure Gage 0 – 100PSI
- Diaphragm Pump

Electrical Components:

- TREK 10/10B high voltage amplifier
- PLC SEL – 2411
- KEITHLEY 6517B
- 2 HEWLETT PACKARD E3612A power supply
- TENMA 72-7925 volt meter
- RIGOL DP1308A power Supply

Optical Components

- Red Lake Motion XTRA HG-XR

The injection chamber was designed to spray one injection and capture the event from the vertical view. A sight glass was installed into the bottom of the chamber where an angled mirror was placed for capturing the event using a high-speed camera. Initial design included a pushbutton valve. See the parts list and solid works model of the initial injection chamber in Appendix B.

After initial testing for repeatability of charge, the push button valve was replaced with an automated valve to increase consistency of injected volume of fuel. A PLC SEL-2411 was used to control the normally closed electric solenoid valve. This allowed for setting the injection delay and injection time. To provide consistent power to the valve the RIGOL DP1308A power supply was used. The initial design had to be modified for use with the acquired high speed camera. Modification included removal of infrared laser, increased diameter base, and drainage modifications. A revised block diagram and SolidWorks model can be seen below.

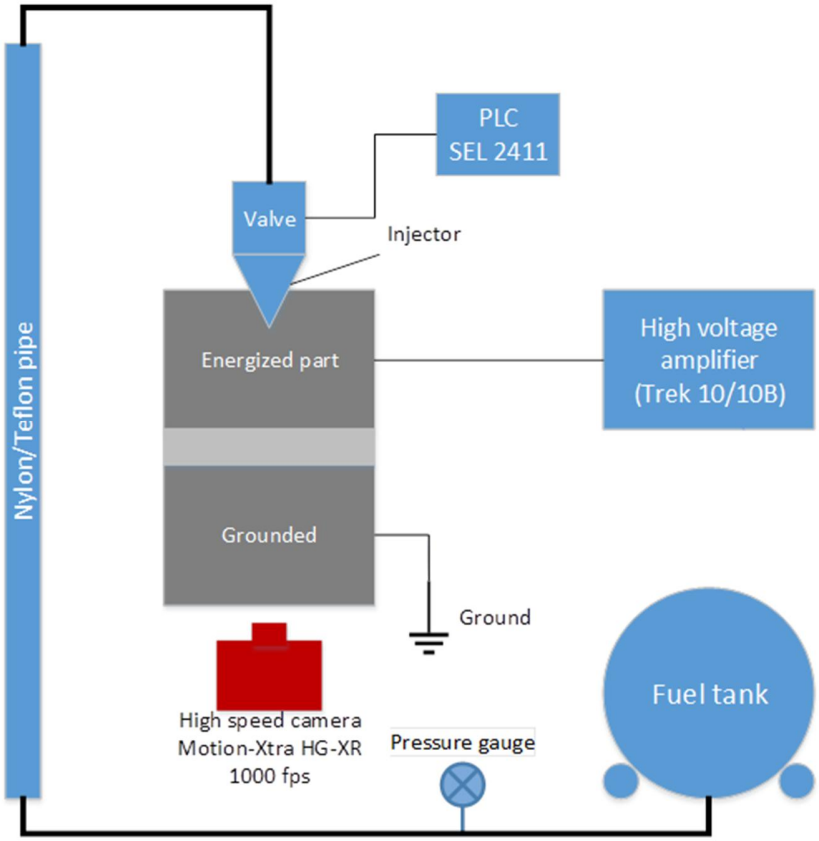

Figure 10: Revised test chamber layout

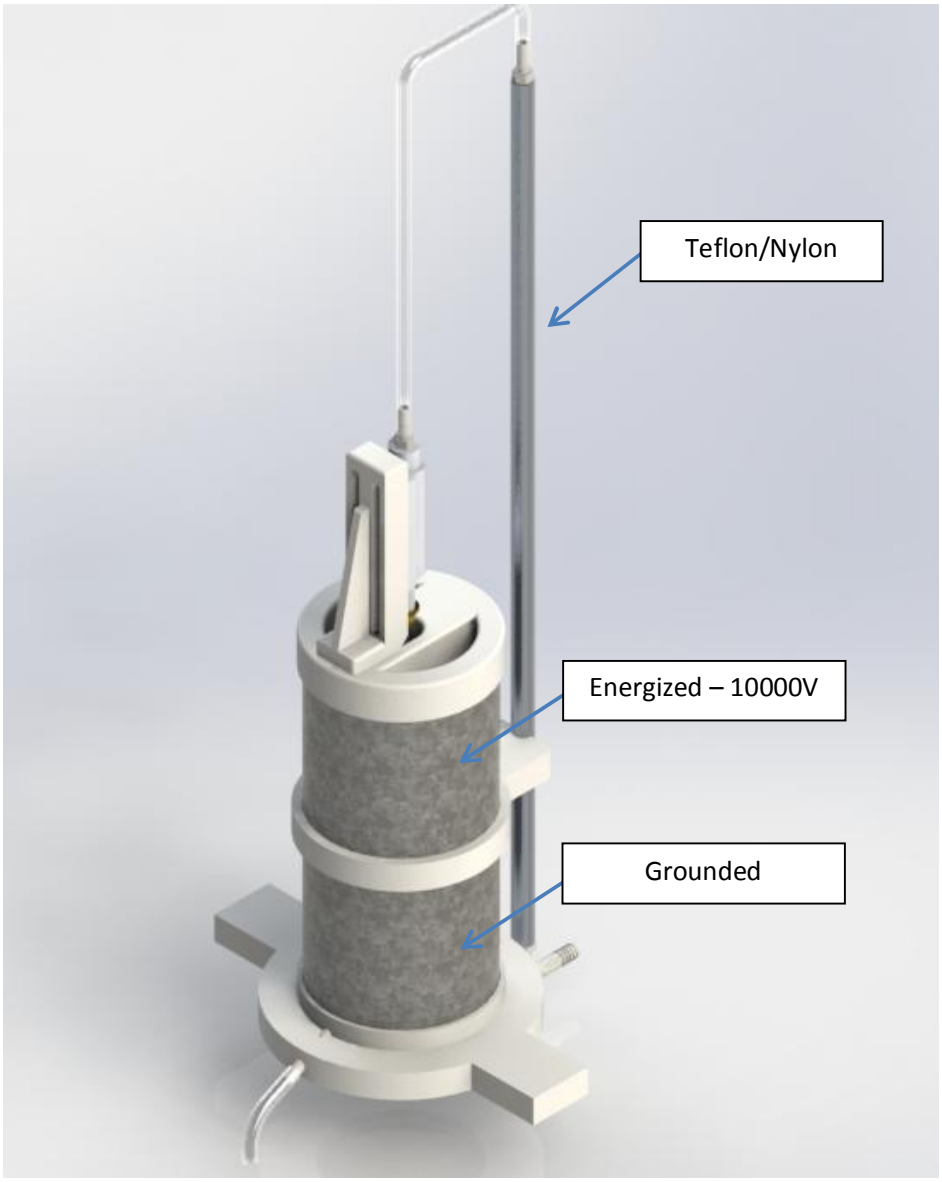

Figure 11: Revised chamber

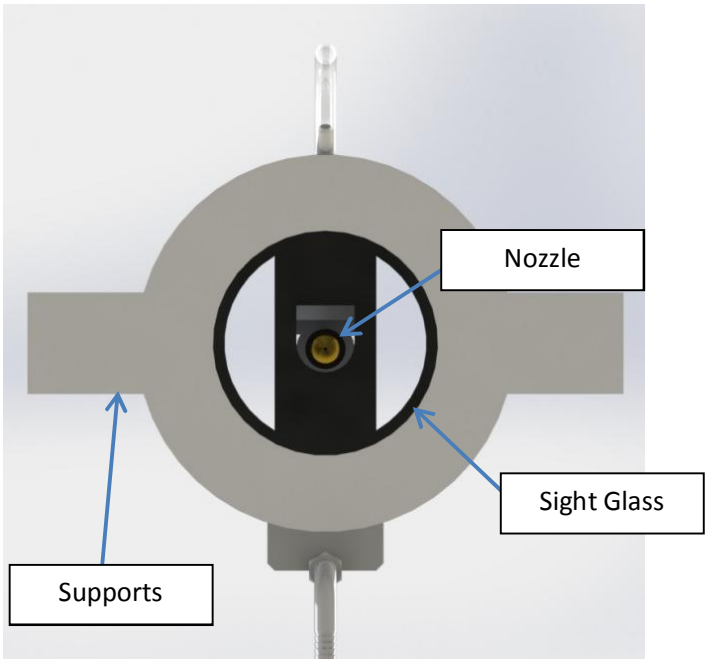

Figure 12: Revised chamber bottom

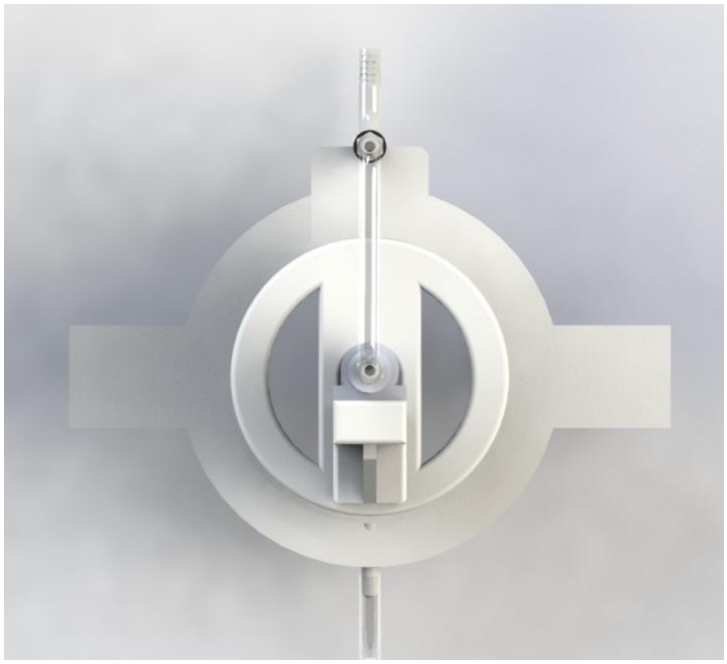

Figure 13: Revised chamber top view

3.5 Testing Definition

The chamber was constructed using 4” diameter pipe cut into two sections. The support dividers and valve mount were 3D modeled and printed out of ABS plastic. All

components associated with the chamber assembly fit together for easy assembly and disassembly. To generate the electric field, the TREK 10/10B high voltage amplifier, capable of applying 10000 V was implemented. The high voltage source uses an amplifier to increase the voltage to 10000 V and is diplayed in Figure 15. The negative connection of the high voltage output was placed on the upper section of the chamber. The ground connection was placed on the lower section of the chamber. This resulted in an application of an electric force to the fuel as soon as it exited the nozzle and entered the cylinder. To capture the injection a Red Lake Motion Xtra HG-XR camera was placed in front of the injection chamber and a mirror was set at an angle to reflect the event. A high intensity light source was used to aid the camera's ability to capture the event. Refer to Figure 14.

Figure 14: Display of testing set up

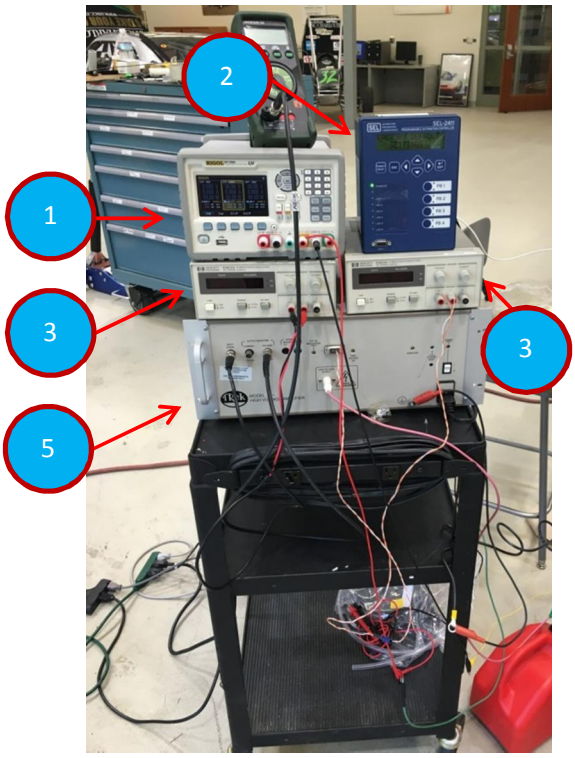

Figure 15: High voltage and SEL equipment

Figure 14 shows the setup of the chamber fixtured to the holding dock. The clamps were used to hold the chamber level for spraying purposes. Figure 15 shows electrical components (1 – RIGOL power Supply, 2- SEL 2411, 3 & 4 – HP power supply, 5 – TREK 10/10B HV amplifier). The high speed camera views the event that is conducted in the chamber by the mirror which is shown in Figure 16. This mirror is placed at an angle under the glass bottom of the cylinder.

Figure 16: Mirror placement

The Red Lake Motion-Xtra HG-XR in Figure 17 was used to capture images at 1000 frames per second during the duration of the injection.

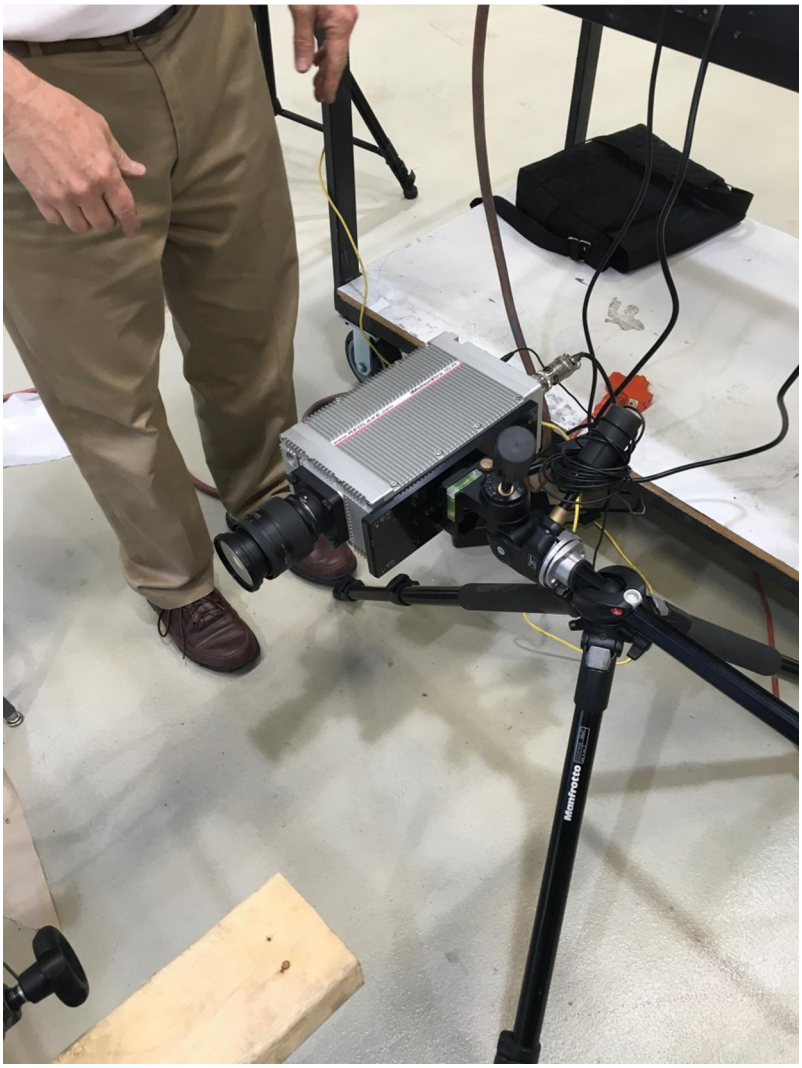

Figure 17: Mounted Red Lake Motion-Xtra HG-XR

After the camera captures the fuel injection, the output can be modified to retain the desired elapsed time of the injection as shown in Figure 18. The files produced were tiff extensions which were used to analyze the process frame by frame for comparison.

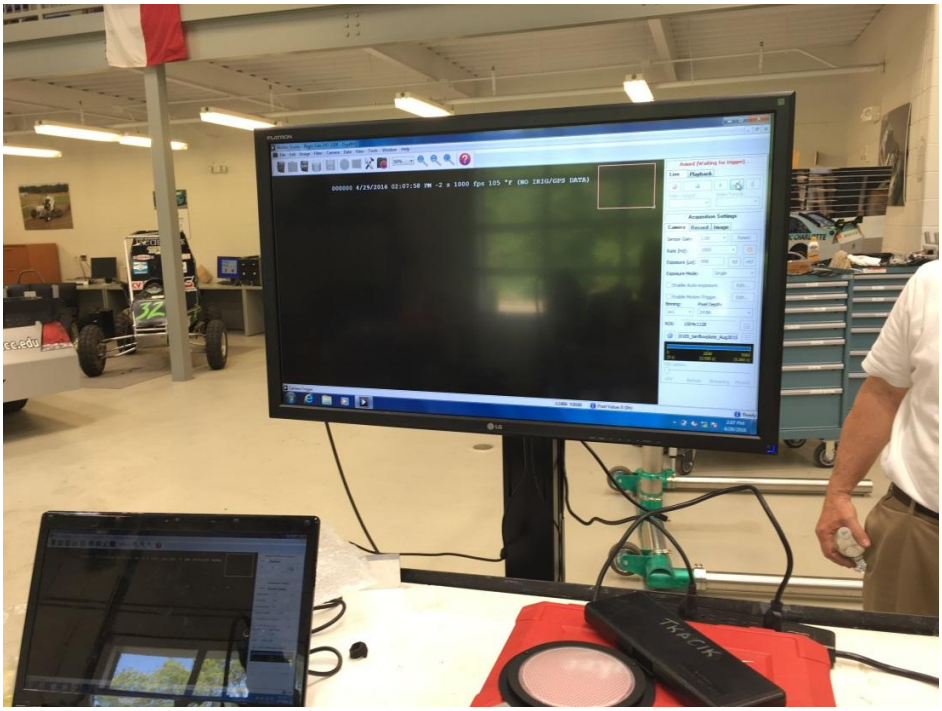

Figure 18: Setup for retention of TIFF files

Motion Studio, supported by Innovation in Motion (IDT) was used to compare the injections. Individual frames were evaluated over the range of injection time. The injection profile shape was analyzed throughout the transition period from the nozzle to the middle section of the chamber. During the recorded amount of frames in which the event took place, eight measurements were taken for each of the four experiments. Measurement distance from the nozzle can be seen in Figure 19 below.

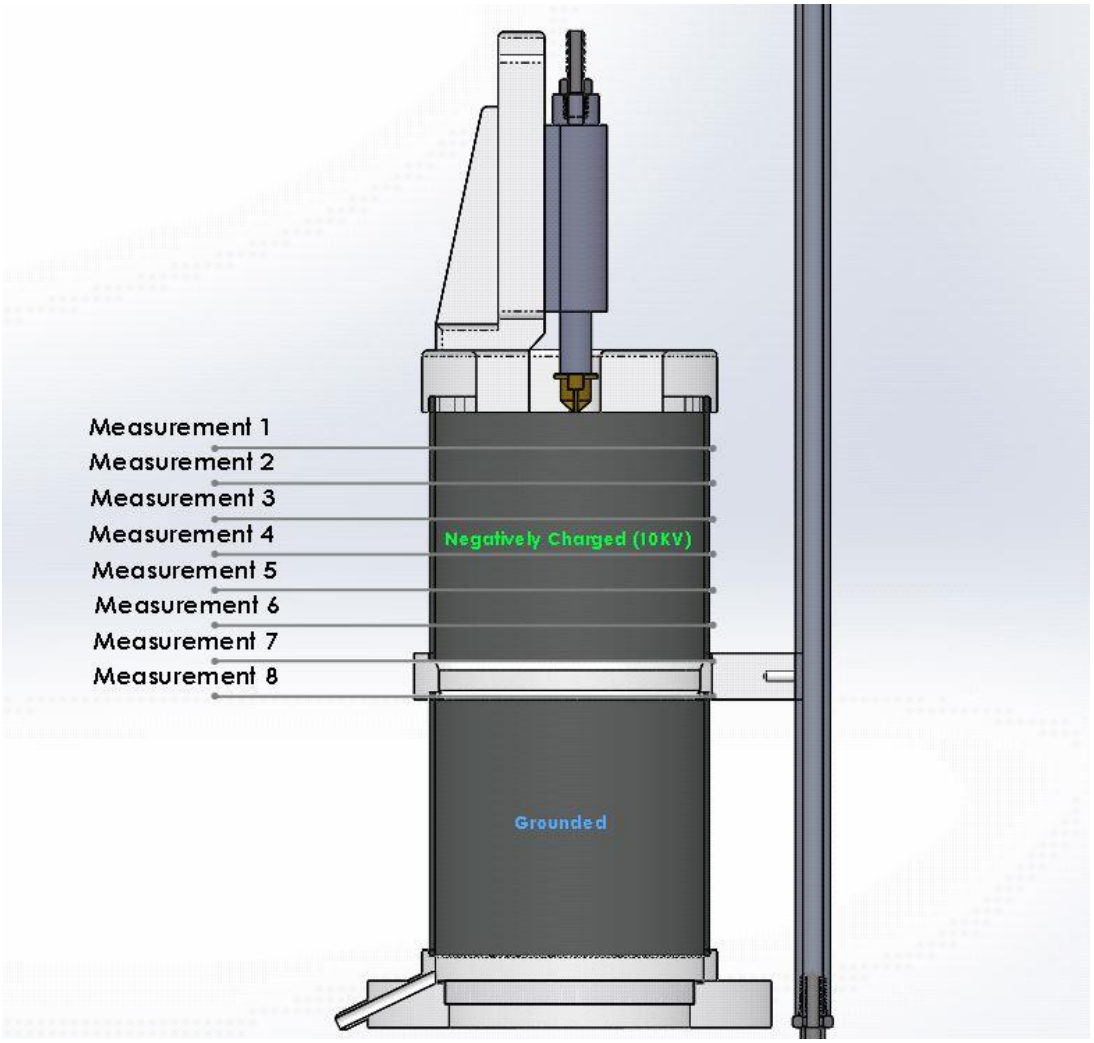

Figure 19: Measurement locations from the nozzle of the injection chamber

CHAPTER 4: RESULTS

4.1. Experimental Results

4.1.1 Charging Repeatability of Dielectrics (Teflon)

The experimental results for repeatability and magnitude showed that the charge applied to the liquid was in the range of -0.1 to -0.4 nC/g. 88.75% of these values for all injection pressures were found to be within +/- 0.05 nC/g from the mean at all four injection pressures. Original equipment included a push button valve where the time of injection was dependent on the operator's ability to maintain a constant spray time. The tubing section for the specified materials was lengthened to increase overall net charge. By increasing the pipe length by one foot, the net charge increased. However, the magnitude increase of the overall net charge was minimal. Theoretically, if the pipe continued to be lengthened the injection charge would continually increase.

An automated valve was installed to maintain a consistent spray time. It was observed that 100% of the values fell within +/- 0.05 nC/g. However, due to more uniform injection times the deviation of the charge magnitudes decreased to -0.1 to -0.3 nC/g. The maximum mean charge density using the auto valve with an injection time of 0.25 seconds was -0.259 nC/g. This value was recorded at 138 kPa using Teflon piping. Refer to Table 2 below for average charge density using an automated valve and a three foot section of charging pipe. Raw data can be seen in APPENDIX C.

Table 2: Average charge density

Injection Pressure	Charge Density of Teflon [nC/g]	Charge Density of Nylon [nC/g]
15	-0.248	-0.236
20	-0.259	-0.225
25	-0.219	-0.185
30	-0.162	-0.165

Figure 20 shows all injection charging averages based on injection pressure and charging material. It shows that the highest magnitude of negative charge was achieved using Teflon at and injection pressure of 138 kPa.

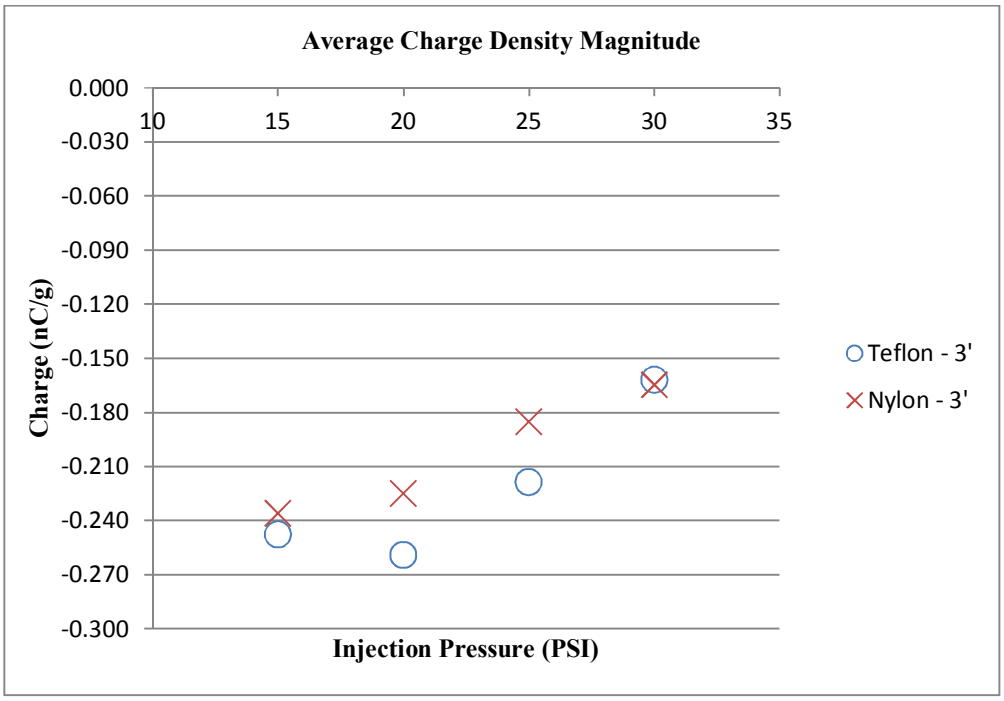

Figure 20: Injection charge density

The overall net charge was evaluated based on the charge density measured using the Faraday cup and the average of 10 separate injections at all four injection pressures. The weight of each injection event was measure using a scale. Refer Figure 21 for a layout of the test setup used.

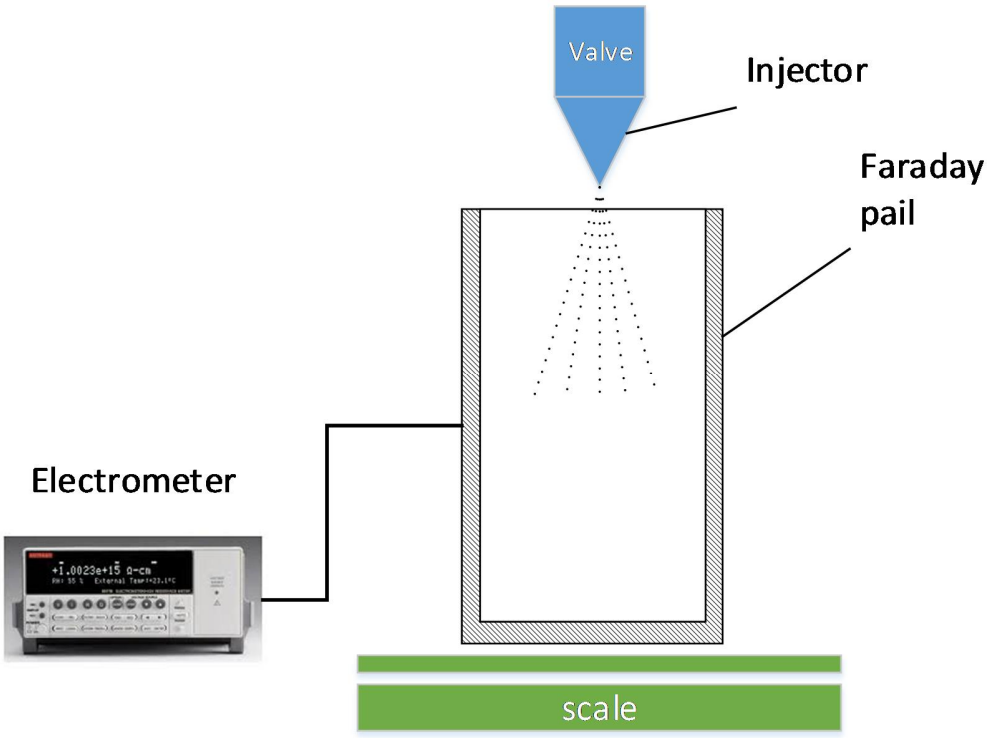

Figure 21: Charging measurements test setup

Experimental results showed that using the automated valve decreased the variation of measured injection weight for each injection. All injection weights fell within +/- 1 gram. Refer to Table 3 below for average injection weights for the auto and push button valve testing. Raw data can be found in APPENDIX D and E.

Table 3: Average Injection Weight in Grams

Injection Pressure	Average Weight Auto Valve [g]	Average Weight Push Button Valve [g]
15	10.61	10.73
20	12.26	11.64
25	13.66	12.88
30	14.48	13.66

4.2 Directional Control of Electrosprayed Fuel

Using 138 kPa with Teflon as the charging material, four injections were tested and results were evaluated. Based on visual observation, some initial effects were determined. They indicated that the fuel particles, when injected into an electric field, were affected by compressing the fuel profile. These initial results were verified by measuring the four injection profiles at the eight locations described in Figure 19 above. In Motion Studio, calibration of the viewing area was conducted using the diameter (110.3mm) of the cylinder as displayed in Figure 22.

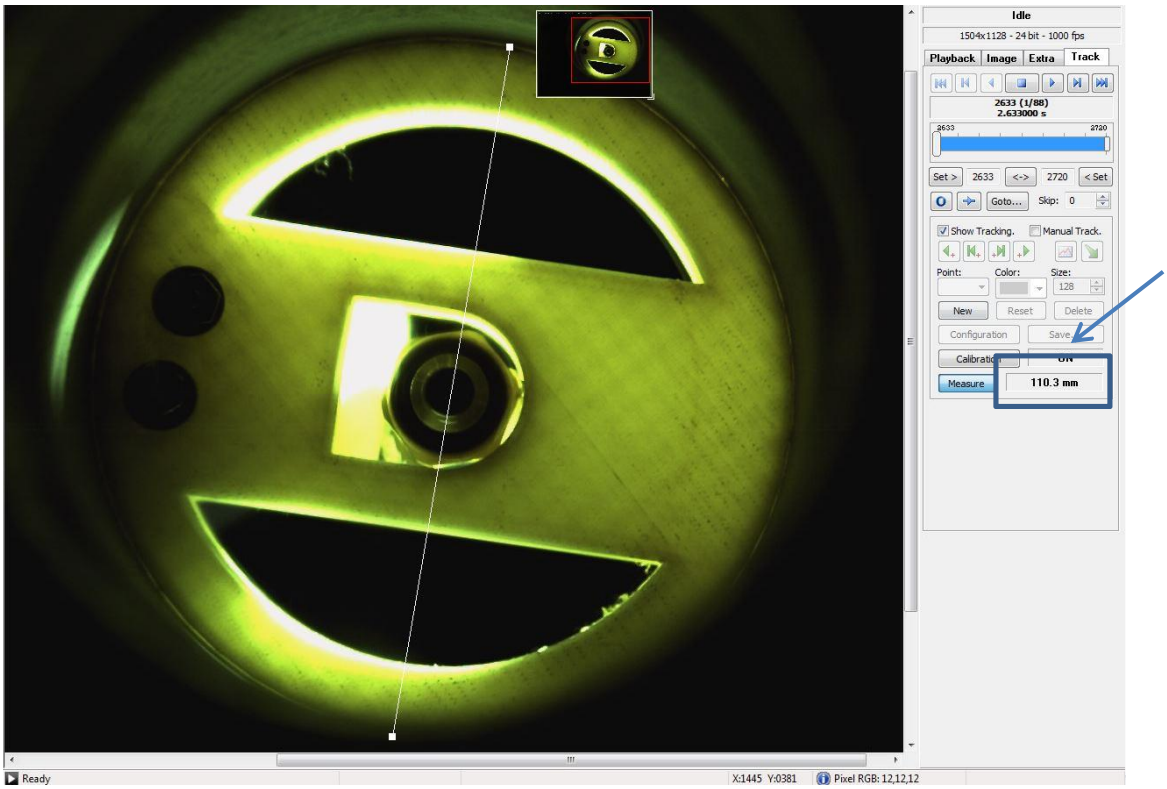

Figure 22: Calibration of the Image for Measurement

Measurement of the fuel profile was determined for both the X and Y directions for all four injections (Injection 1 – No electric field applied, Injection 2 – Electric field applied kV, Injection 3 – No electric field applied, Injection 4 – Electric field applied 10 kV). The initial diameter of the fuel profile was measured after it left the nozzle as shown

in Figure 23. The radial measurement seen below is for injection 2. These measurements were repeated for all four injections. This profile definition was taken at a distance of 14.5 mm from the injection nozzle.

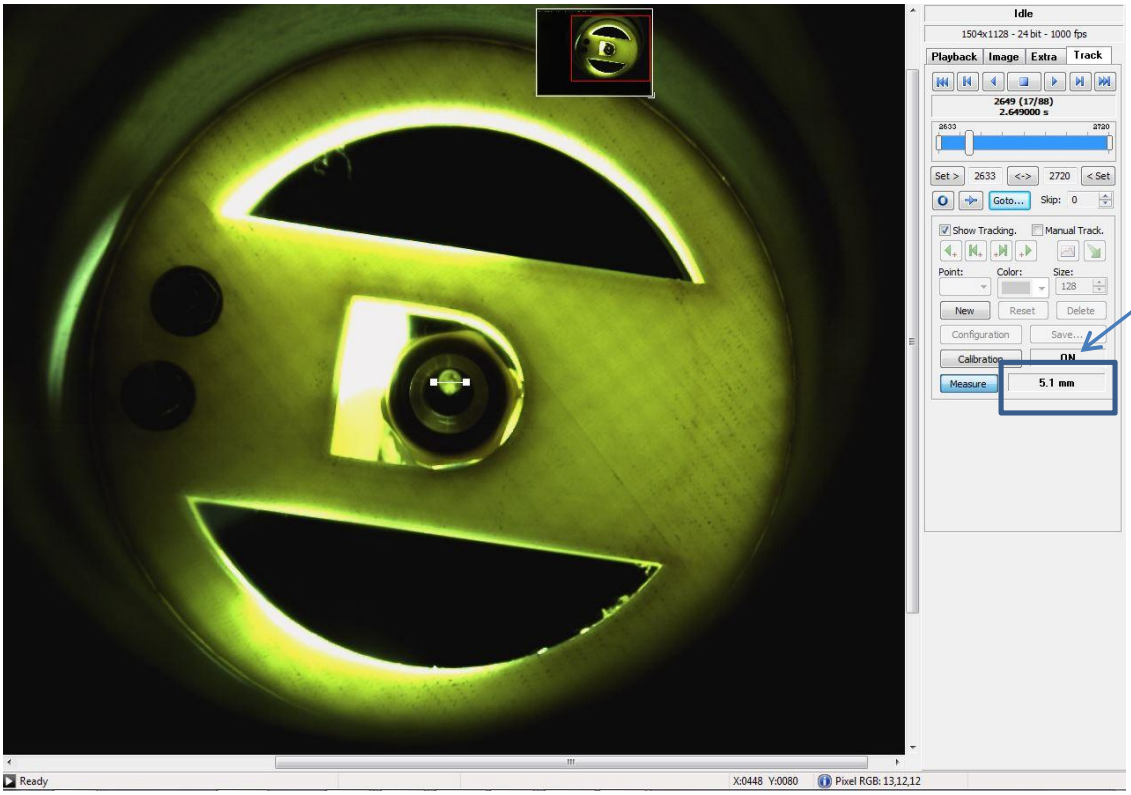

Figure 23: First measured distance of fuel in the X direction

To locate the eight measurement locations from the nozzle for all four injections, the overall injection duration for the time period when the fuel left the nozzle until it hit the glass stock at the bottom was found. Then individual frames were determined based on the overall height of the chamber. Each distance of measure from the nozzle was determined and the specific frame at this distance was specified for all four of the individual injections. The velocity for each injection was estimated using the elapse time of the event based on the chamber height from the nozzle exit to the glass stock face. The average velocity was 14.3 m/s. Refer to APPENDIX F for the frame definition and

estimated velocities. Figure 24 shows the last measurement in which the fuel was taken and deemed relevant before the fuel entered the lower half of the chamber which is grounded and no longer experiencing forces seen from the negatively charged electric field. This measurement was taken at 116.2 mm from the nozzle exit.

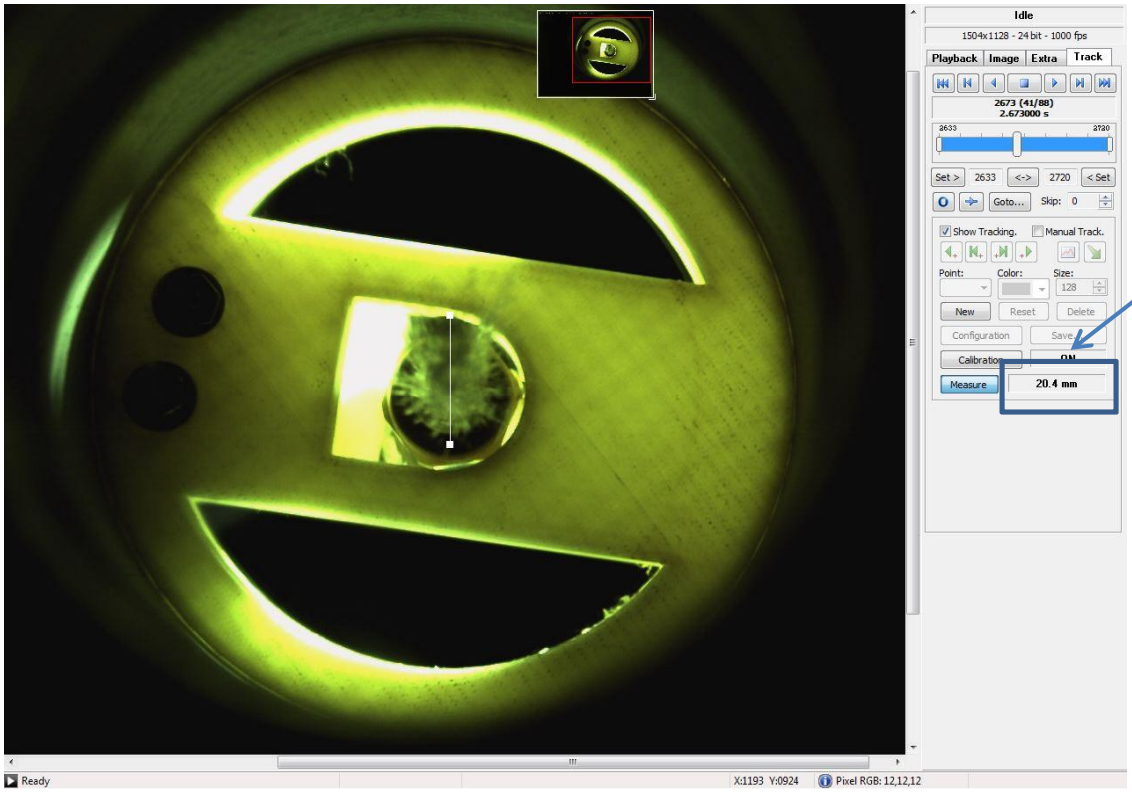

Figure 24: Last measurement position in the Y direction

For each direction control test, the injection pressure was 138 kPa and the test was conducted at a room temperature of 297 K. All X and Y measurements for the four different injections are represented in Tables located in APPENDIX G. To demonstrate a clear visual of how the entrainment of the fuel was achieved, Solid Works was used to regenerate 3D fuel profiles based on the measurements of the X and Y direction for all four test injections. Each injection Profile was reconstructed by sketch planes at the eight distances from the nozzle to show the transitional fluid flow for the top section of the chamber. Injection models were then mated in the assembly to compare the width of the

profiles and to give a visual of the compression of the fuel cloud with and without the electric field applied. Figure 25 below shows the comparison of the reconstructed injecting profile for tribocharged fuel with and without the applied electric field. It is clear that the fuel profile for injections 2 and 4 is radially controlled when applying a -10 kV potential to the top section of the chamber. The directional control in the x direction can be seen visually when comparing the overall dynamic fluid flow.

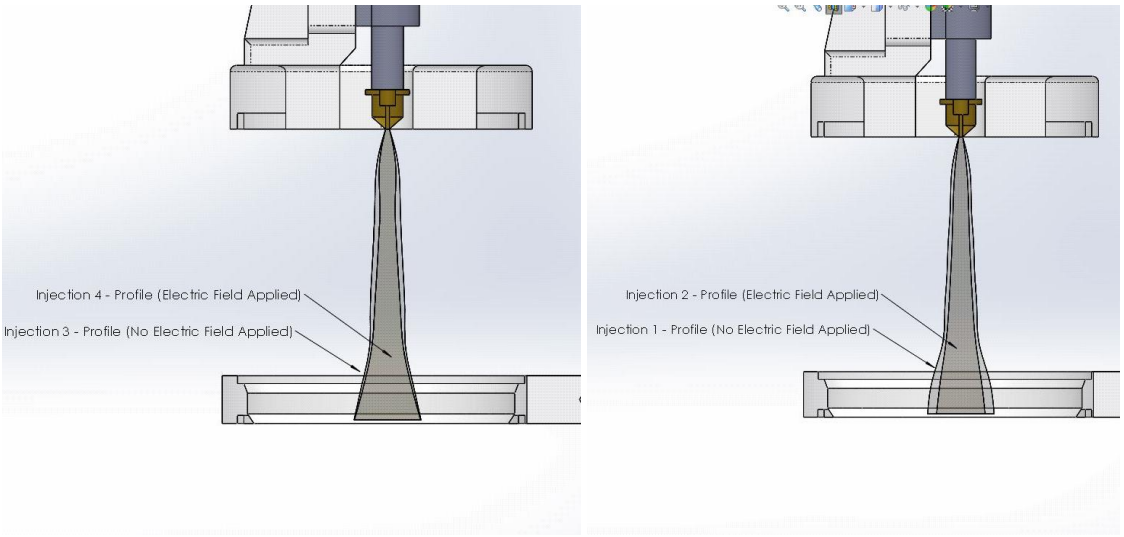

Figure 25: Injection comparison (1 to 2) & (3 To 4)

To further investigate that the fuel profile was controlled radially for both, electric field and non-electric field cases, injections 1 & 4 were compared and injection 2 & 3 were compared. Similar results were seen that fuel cloud was compressed when applying the electric field by charging the chamber. The last comparison investigated for validation purposes was the profile similarities of the two cases at the same injection characteristics and environmental conditions. Profile similarities are evident when overlaying the profiles. This verifies that the measurements taken are accurate due to the profiles having the same trajectories when injected into the chamber at the same

conditions. Refer to Figure APPENDIX H for a visual representation of the injection comparison.

4.3 Electrostatic and Fluid Dynamics Simulation Investigation

4.3.1 COMSOL Multiphysics Uniform Droplet Size Simulation

Preliminary exploration was completed using FEA software Comsol Multiphysic. A model was constructed to simulate the results of pressurized injections of electro-sprayed fuel into an atmospheric cylinder with and without an electric field applied. These models (Test 1 and Test 2) were used to demonstrate the dynamic movement of the fluid created by the electric fields inside of the chamber. The spray chamber geometry consisted of a two section cylinder that represented the designed spray chamber for injection testing. The separate sections were used to create the alternating charge to repel the fuel droplets for the test case inducing the electric field. Using the built in physics electrostatics, an electro potential charge was applied to the top of the cylinder wall respectively. Particle tracing was implemented to simulate the injected fuel with an applied negative charge based on testing data. To simplify the model some assumptions were made. The droplet diameter was assumed to be uniform and the number of droplet generated was set at 50 for the first simulation test. All droplets released from the grid were set at a diameter of 5μm.This minimized complexity and improved simulation execution time.

4.3.1.1 Test Case 1 – No Electric Field Applied to the Chamber

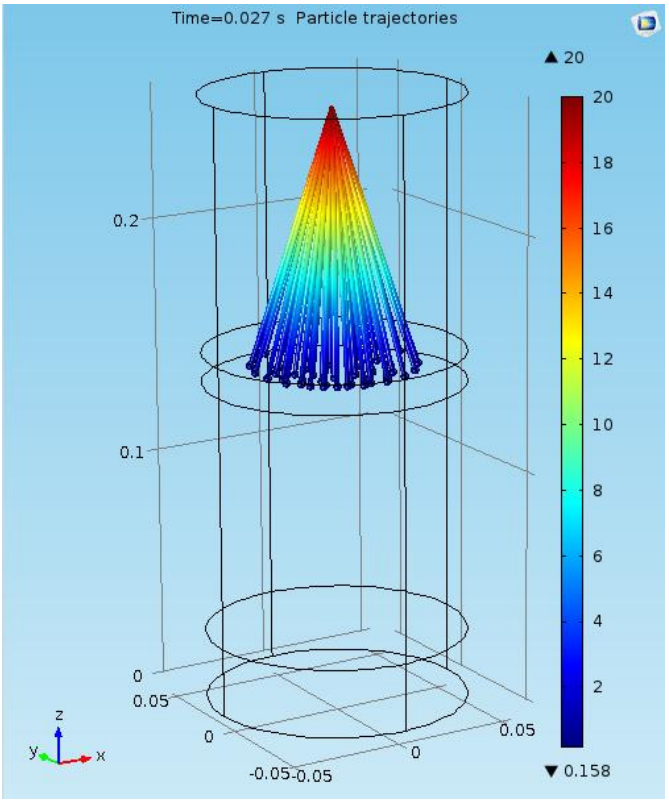

Figure 26: COMSOL particle trajectories test case 1

The results, as seen in Figures 26 show the particle trajectories based on a zero charge potential inside of the chamber. Penetration after 27ms reaches approximately 0.75 m from the release point at z = 0.25 m. A total of 50 symmetrical droplets are injected at a cone angle of 30°. The droplets size was assumed to stay constant for simplification purposes. The velocity associated with the initial spray approaches 0 m/s stopping the fluid from further penetration inside of the cylinder. Test Case 2 was then simulated utilizing the same parameters for comparison of implemented technology. Refer to APPENDIX I for definition of parameters imported for testing.

4.3.1.2 Test Case 2 – Electric Field Applied to the Chamber

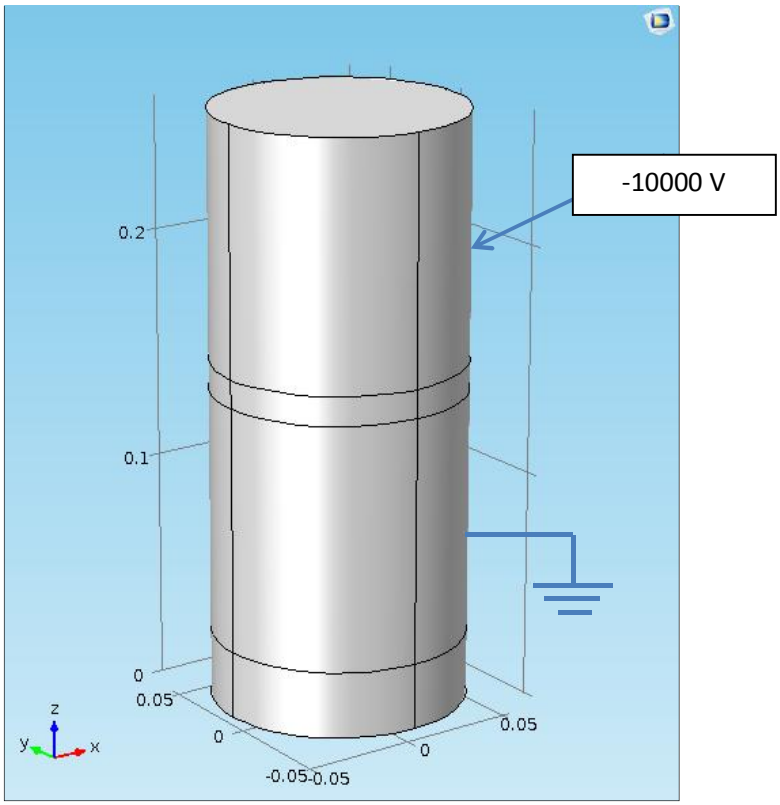

Figure 27: COMSOL defined geometry test case 2

The geometry seen in Figure 27 shows the two separate cylinders constructed within the parameters used for the original non-charged model. An analytical expression was developed within the time interval of 27 ms to simulate a charge of -10,000 V and was applied to the top section of the cylindrical geometry. The bottom section of the chamber was grounded.

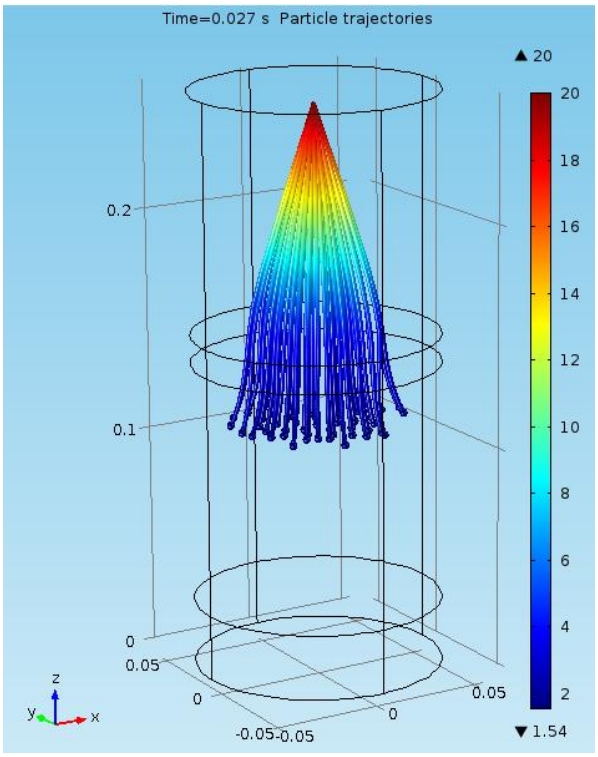

Figure 28: COMSOL particle trajectories test case 2

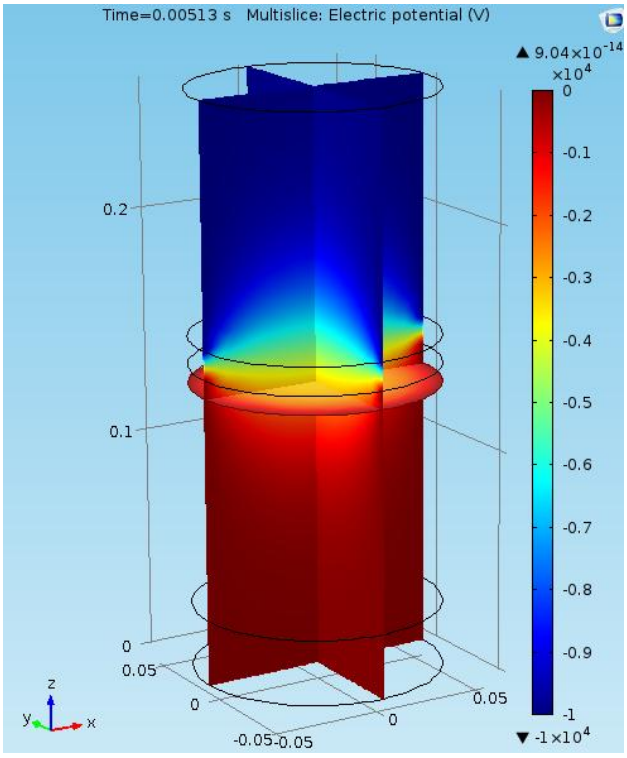

Figure 29: COMSOL electric potential test case 2

Integrating the same spray parameters seen in the first simulations resulted in Figures 28 and 29. They demonstrate the effect on penetration and trajectory of the fuel particles after 27ms while applying the analytical constraint to generate an electric field. Testing data for charge magnitude was used to estimate the charge applied to the individual fuel droplets. The penetration increases to approximately 0.15 m from the point of release at Z=0.25 meters. The electric potential was applied for the top section of the cylinder where the voltage applied is -10000 V. These results showed that with the charge applied to the fuel droplets trajectory can be manipulated in the x and y direction radially when injecting them into an electric field.

4.3.2 COMSOL Multiphysics Non-uniform Droplet Size Simulation

The simulation model was adapted to include non-uniform droplet sizes. A normally distributed range was implemented into the above simulation and random diameter sizes were generated for the 50 droplets released. The range for the diameter was set to include 99% of the deviated size over the normally distributed curve. Figure 30 and 31 below shows the distribution for the diameter size and the charge applied based on the diameter of the 50 droplets generated respectably.

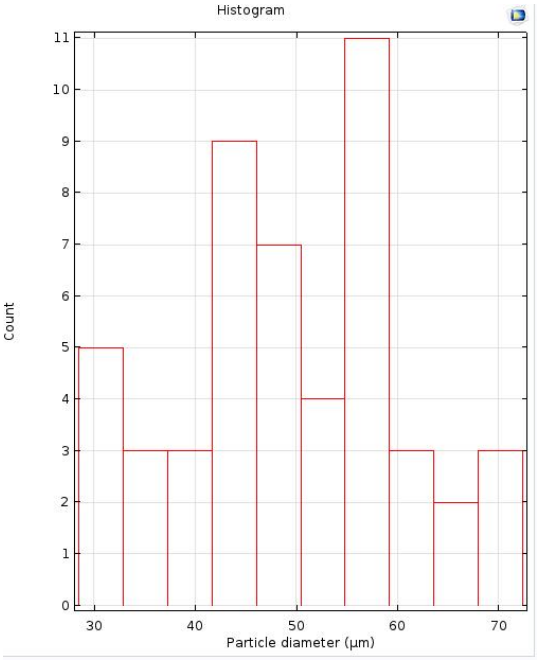

Figure 30: Distibution of Droplet Size

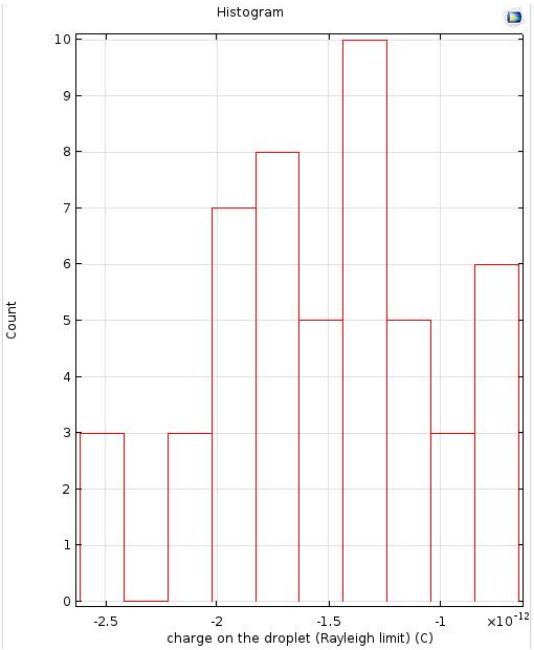

Figure 31: Charge of the droplets

Both simulations were computed for a 0 V and -10000 V potential applied to the top section of the chamber. Results showed that with no potential applied, the droplets injected into the cylinder reach different depths. This is due to the drag force affecting the smaller droplets differently than the larger droplets. When the negative potential is applied, the droplets are manipulated entraining the profile and displacing the droplets to increase the depth penetration. Refer to Figures 32 and 33

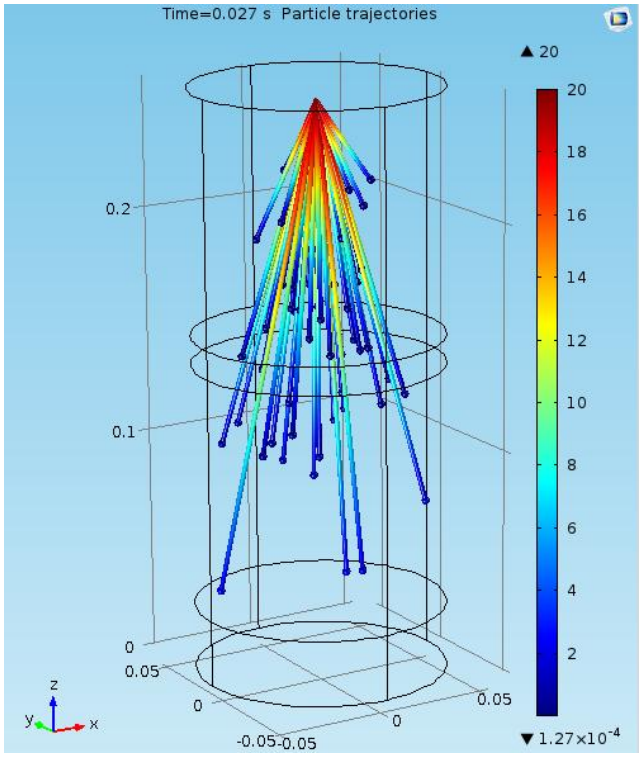

Figure 32: COMSOL particle with no potential applied

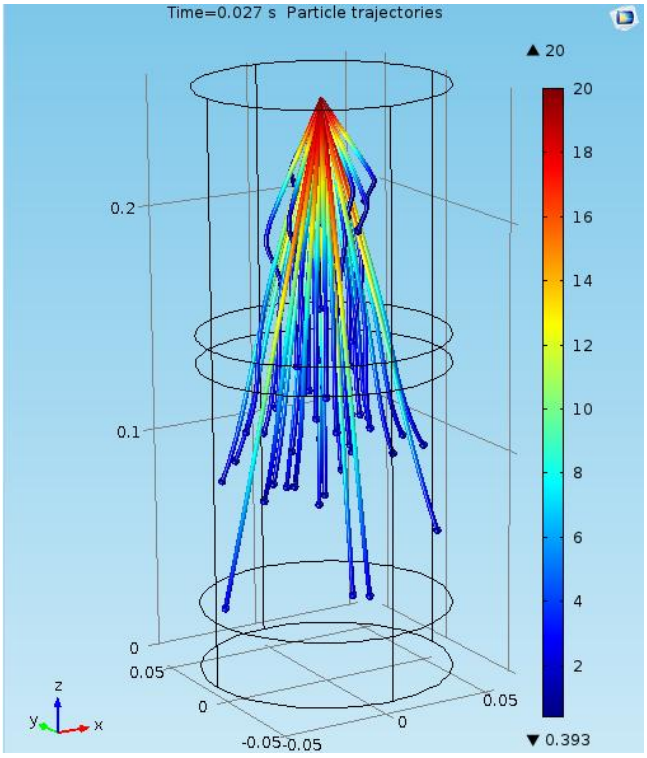

Figure 33: COMSOL particle with -10 kV applied

CHAPTER 5: CONCLUSIONS

5.1 Discussion

The process of charging a dielectric fluid (gasoline) at injection pressures of 103, 138, 172, and 207 kPa using no external source was achieved by selecting material with tribocharging characteristics. Teflon and nylon have been used for electrospraying and proven to provide good charging characteristics for powders. Therefore, both materials were tested for charging capability of a dielectric liquid gasoline.

Experimental results showed that the repeatability of charging this liquid included a range of 100% of the values falling within +/- 0.05 nC/g. This was achieved by replacing the original push button valve with an automated normally closed electrical driven valve. Magnitude of charge over the injection pressure ranged from a maximum charge of -0.259 nC/g and -0.225 nC/g at 20PSI to a minimum of -0.162nC/g and -0.165 nC/g for teflon and nylon respectively Increasing the length of the pipe increased the overall net charge of the fuel injected. However, by increasing the pipe by one foot the charge increase was minimal at an average of -0.059 nc/g. After analyzing the charging results it was concluded that the maximum charge was achieved when using teflon at 20 PSI.

Tests for control over the injected profile for the charged fuel was investigated for four different test injections at 20 PSI due to the charging results (Injection 1 – no electric field applied, Injection 2 – electric field applied 10K, Injection 3 – no electric field applied, Injection 4 – electric field applied 10K). Comparison was achieved by taking x and y measurements at eight different frame intervals during injection. Frames were accrued at 1000 FPS at a vertical observation angle. Compression of the injection event was achieved over the charged section of the chamber.

Maximum displacement was found to be 1.7mm radially for the x direction and 3.7 mm in the y direction for injections 1 and 2. Maximum displacement for the comparison of injection 3 and 4 in the x and y direction was 0.9mm and 2.0mm respectively. All testing was completed at atmospheric pressure. These results show that the overall compression of the electro sprayed fuel can be achieved at atmospheric pressure. However, results are seen not to be perfectly symmetrical for different injection events. This could be a result of slightly different injection pressures and the formation of different droplet diameters. Basic fluid dynamics demonstrate that the overall sizes of the fuel droplets are controlled by the electrical forces in the horizontal direction. The inertia of the moving droplet is altered by applying an electric field to the injected environment. This entrainment was achieved with minimal charging to the fluid.

5.2 Possible Future Work

This investigation looks promising for the control and entrainment of the fuel profile using electric fields. However, this test setup was investigated at a minimum pressure for the injection chamber. Continued research is required to validate the

investigation of high pressure charged injection into a pressurized injection chamber. Possible expansion of the work could include:

- Charging fuel using the tribocharging method at high injection pressures
- Injection control of electrosprayed fuel in a high pressure environment
- Increased Electric field optimization of compressing the injection profile
- The investigation of controlling charged diesel fuel in an electric field chamber
- The investigation of applying magnetic field to control the movement of the charged dielectric fluid
- The control of injection to combustion of combustible fluids using electric fields

BIBLIOGRAPHY

[1] G. W. G. S. M. Pitcher, "Velocity and Drop Size Measurements in Fuel Sprays in a direct injection diesel engine," *PPSC Particle & Particle Systems Characterization,* vol. 7, pp. 160-168, 1990.

[2] K. S. Varde and T. Watanabe, "Characteristics of High Pressure Spray and Exhaust Emissions in a Single Cylinder DI Diesel Engine," presented at the Fisita World Automotive Congress, Seoul, Korea, 2000.

[3] J. Zeleny, "The Electrical Discharge from Liquid Points, and a Hydrostatic Method of Measuring the Electric Intensity at Their Surfaces," *Physical Review,* vol. 3, pp. 69-91, 02/01/ 1914.

[4] J. S. Shrimpton, "Pulsed charged sprays: application to DISI engines during early injection," *International Journal for Numerical Methods in Engineering,* vol. 58, pp. 513-536, 2003.

[5] E. L. Keating, *Applied combustion*. Boca Raton: CRC Press/Taylor & Francis, 2007.

[6] S. McAllister, J.-Y. Chen, and A. C. Fernandez-Pello, "Droplet Evaporation and Combustion," in *Fundamentals of Combustion Processes*, ed New York, NY: Springer New York, 2011, pp. 155-175.

[7] G. Fiengo. (2013). *Common rail system for GDI engines modelling, identification, and control*. Available: public.eblib.com/choice/publicfullrecord.aspx?p=1030337

[8] U. Leuteritz, A. Velji, and E. Bach, "A Novel Injection System for Combustion Engines Based on Electrostatic Fuel Atomization," *SAE International,* 2000.

[9] L. Li, S. Yu, and Z. Hu, "Theoretical and experimental studies of electrospray for IC engine," in *2006 SAE World Congress, April 3, 2006 - April 6, 2006*, Detroit, MI, United states, 2006.

[10] E. K. Anderson, D. C. Kyritsis, A. P. Carlucci, and A. De Risi, "Electrostatic effects on gasoline direct injection in atmospheric ambiance," *Atomization and Sprays,* vol. 17, pp. 289-313, 2007.

[11] E. Anderson, D. Kyritsis, R. Coverdill, and C.-F. Lee, "Experimental evaluation of electrostatically assisted injection and combustion of ethanol-gasoline mixtures for automotive applications," in *SAE 2010 World Congress and Exhibition, April 13, 2010 - April 13, 2010*, Detroit, MI, United states, 2010.

[12] D. Kim and P. Moin, "Numerical Simulation of the Breakup of a round liquid jet by a coxial flow of gas with a subgrid Lagrangian breakup model," 2011.

[13] G. Zhang, X. Qiao, X. Miao, J. Hong, and J. Zheng, "Effects of highly dispersed spray nozzle on fuel injection characteristics and emissions of heavy-duty diesel engine," *Fuel,* vol. 102, pp. 666-673, 12// 2012.

[14] J. Hancsók and S. P. Srivastava. (2013). *Fuels and fuel-additives*. Available: public.eblib.com/choice/publicfullrecord.aspx?p=1598818

[15] H. L. Nguyen, "Two-Dimensional Analysis of Two-Phase Reacting Flow in a Firing Direct-Injection Diesel Engine," NASA, Ed., ed, 1989.

[16] S. Tchung-Ming, "Transport energies: advantages and disadvantages," 2009.

[17] A. K. Agarwal, D. K. Srivastava, A. Dhar, R. K. Maurya, P. C. Shukla, and A. P. Singh, "Effect of fuel injection timing and pressure on combustion, emissions and performance characteristics of a single cylinder diesel engine," *Fuel,* vol. 111, pp. 374-383, 9// 2013.

[18] N. Chigier, "Challenges for future research in atomization and spray technology arthur lefebvre memorial lecture," in *10th International Conference on Liquid Atomization and Spray Systems, ICLASS 2006, August 27, 2006 - September 1, 2006*, Kyoto, Japan, 2006, pp. International Institute of Liquid Atomization and Spray Systems; Institute for Liquid Atomization and Spray Systems - ASIA; Institute for Liquid Atomization and Spray Systems - Americas; Institute for Liquid Atomization and Spray Systems - Europe; The Japan Institute of Energy.

[19] T. Watanabe, S. Daidoji, and K. S. Varde, "Relationship between visible spray observations and DI diesel engine performance," *Journal of Engineering for Gas Turbines and Power-Transactions of the Asme,* vol. 122, pp. 596-602, Oct 2000.

[20] J. Shrimpton, *Charge injection systems : phycical principles, experimental and theoretical work*. Berlin: Springer Verlag, 2009.

[21] B. G. Prajapati and M. Patel, "Electro Spray Technology," *A Technology Update,* vol. 1, 2010.

[22] F. A. International Colloquium in Textile Engineering, Design, M. R. Ahmad, and M. F. Yahya. (2014). *Proceedings of the International Colloquium in Textile Engineering, Fashion, Apparel and Design 2014 (ICTEFAD 2014)*. Available: http://dx.doi.org/10.1007/978-981-287-011-7

[23] H. Baharvand and N. Aghdami. (2014). *Stem cell nanoengineering*. Available: public.eblib.com/choice/publicfullrecord.aspx?p=1895482

[24] J. M. López-Herrera, A. Barrero, A. Boucard, I. G. Loscertales, and M. Márquez, "An experimental study of the electrospraying of water in air at atmospheric

pressure," *J Am Soc Mass Spectrom Journal of the American Society for Mass Spectrometry,* vol. 15, pp. 253-259, 2004.

[25] "Electrospray for fuel injection," *Automotive Engineering,* vol. 106, 1998.

[26] A. Gomez and K. Tang, "Charge and fission of droplets in electrostatic sprays," *Physics of Fluids,* vol. 6, pp. 404-14, 01/ 1994.

[27] S. Yu and Z. Hu, "Theoretical and Experimental Studies of Electrospray for IC Engine," *SAE International,* 2006.

[28] H. M. A. Elghazaly and G. S. P. Castle, "Experimental study on the breakup of charged liquid droplets," *Industry Applications, IEEE Transactions on,* vol. 25, pp. 48-53, 1989.

[29] M. B. Mayr, S. A. Barringer, U. Ohio State, S. Department of Food, and Technology, "Corona vs triboelectric charging for electrostatic powder coating," 2005.

[30] T. Paillat, E. Moreau, and G. Touchard, "Space charge density at the wall in the case of heptane flowing through an insulating pipe," *Journal of Electrostatics,* vol. 53, pp. 171-182, 8// 2001.

[31] E. Németh, V. Albrecht, G. Schubert, and F. Simon, "Polymer tribo-electric charging: dependence on thermodynamic surface properties and relative humidity," *Journal of Electrostatics,* vol. 58, 2003.

[32] A. G. Bailey, "The science and technology of electrostatic powder spraying, transport and coating 1 This invited paper is in commemoration of Prof. Bill Bright who contributed so much to electrostatics and especially to powder coating both directly and by stimulating numerous researchers in this field. 1," *ELSTAT</cja:jid> Journal of Electrostatics,* vol. 45, pp. 85-120, 1998.

[33] R. C. S. J. H. Flagan, *Fundamentals of air pollution engineering*. Englewood Cliffs, N.J.: Prentice Hall, 1988.

APPENDIX A: INITIAL INVESTIGATION OF CONTROLLING ELECTRICALLY CHARGED FUEL DROPLETS USING ELECTRIC FIELDS CALCULATION MATLAB CODE

```
%% Computation of the particle velocity and traveled distance
clear all;
close all;
clc;

%% gasoline parameters
Density_mass=750; %kg/m^3
eta=0.0258 %N/m surface tension at 20 deg. C

%% Particle (droplet) data
Diameter=5e-6 %m
Volume=4/3*pi*(Diameter/2)^3 %m^3
mp=Density_mass*Volume %kg

%% compute tau constant
viscosity=18.47e-6 %Pa*s, air at 297 K and .101 MPa
a=Diameter/2 %m, droplet radius
tau=6*pi*viscosity*a % droplet constant
tm=mp/tau %time constant
Qnet = 3.10e-10 * (1/1000) %Coulombs/kg, Net Charge of Injection
Profile
qD = Qnet*mp
q=8*pi*sqrt(8.85e-12*eta*a^3)%Coulombs, charge of the droplet

%% velocity toward wall
u0=5 %m/s given value

%% plotting velocities for E values
t=linspace(0,1e-3,1000); %time vector 0 to 1 ms, 1000 datapoints
%t=linspace(0,0.027,9)
figure
E=0 % V/m, electric field
u=-q*E/tau*(1-exp(-t./tm))+u0*exp(-t./tm); %velocity
plot(t,u,'k')
hold on;
E=10000 %V/m, electric field
u=-q*E/tau*(1-exp(-t./tm))+u0*exp(-t./tm);
plot(t,u,'g')
xlabel('time, [s]')
ylabel('velocity, [m/s]')
E=100000 %V/m, electric field
u=-q*E/tau*(1-exp(-t./tm))+u0*exp(-t./tm);
plot(t,u,'b')
grid on
legend('E = 0 [V/m]','E = 1 [kV/m]','E = 100 [kV/m]')
%legend('E = 0 [V/m]','E = 100 [kV/m]')
title(strcat('Particle Diameter=',num2str(Diameter),' [m], Particle
Velocity Toward Wall'))
```

```
%% plotting displacements for E values
figure
E=0
x=(-q*E)/tau*(t-tm*(1-exp(-t./tm )))+u0*tm*(1-exp(-t./tm));
plot(t,x*1000,'k')
hold on;
E=10000
x=(-q*E)/tau*(t-tm*(1-exp(-t./tm)))+u0*tm*(1-exp(-t./tm));
plot(t,x*1000,'b')
E=100000
x=(-q*E)/tau*(t-tm*(1-exp(-t./tm)))+u0*tm*(1-exp(-t./tm));
plot(t,x*1000,'g')
legend('E = 0 [V/m]','E = 1 [kV/m]','E = 100 [kV/m]')
%legend('E = 0 [V/m]','E = 100 [kV/m]')
grid on
xlabel('time, [s]')
ylabel('traveled distance toward the wall, [mm]')
title(strcat('Particle Diameter=',num2str(Diameter),' [mm], Distance
Traveled Toward Wall'))
```

APPENDIX B: PARTS LIST AND INITIAL INJECTION CHAMBER DESIGN

Table 4: Parts list

Part #	Part Description	Provider	Length	Quantity	Cost	Total Cost
475-B	Solo BackPack Sprayer	Amazon	-	1	$103.70	$103.70
44555K161	Fuel Pressure Gage Fitting 1/4" Tubel ID x 1/8 Male	McMaster Carr	-	1	$6.86	$6.86
3795K14	Pressure Gage 0-100PSI	McMaster Carr	-	1	$54.99	$54.99
4452K111	1/8 Pipe Size Coupling	McMaster Carr	-	1	$3.36	$3.36
5670K13	Reduction Barbed 3/8" to 1/4"	Mcmaster Carr	-	1	$2.31	$2.31
53505K63	Fitting 1/8" to 1/4"	McMaster Carr	-	1	$11.37	$11.37
51205K471	Fitting 1/8" to 1/8"	McMaster Carr	-	1	$7.63	$7.63
5670K94	90 Degree Elbow 1/4" to 1/8" NPT	McMaster Carr	-	1	$7.88	$7.88
5345K72	Gasket	McMaster Carr	-	1	$6.09	$6.09
8477K29	Glass Stock 3/8"	McMaster Carr	-	1	$36.75	$36.75
62805K46	Leveling Feet 1/2" - 13	McMaster Carr	-	4	$8.53	$34.12
8547K31	Teflon Tube	McMaster Carr	5'	3	$8.66	$25.98
90475A140	1/2"-13 Thin Hex Nuts	McMaster Carr	-	1	$7.69	$7.69
6519T13	ID 1/4 OD 3/8 Ultra-Chemical-Resistant	McMaster Carr	10'	10	$3.30	$33.00
8628K27	Nylon Tube	McMaster Carr	5'	1	$10.56	$10.56
4568T24	6063 Aluminum Rod	McMaster Carr	6'	1	$15.08	$15.08
6790T42	Brass Push Valve 1/8"	McMaster Carr	-	1	$18.48	$18.48
7126K19	EMT Conduit 4"	McMaster Carr	5'	1	$48.24	$48.24
VLM-650-28	Red Laser Line Generator	Amazon	-	1	$25.80	$25.80
51545K83	90 Degree Elbow Quick Disconnect	McMaster Carr	-	2	$ 5.11	$ 10.22
51545K62	Quick-Disconnect Tube Coupling Barbed	McMaster Carr	-	3	$ 11.28	$ 33.84
51545K65	Quick-Disconnect Tube Coupling 1/8 Male NPT	McMAster Carr	-	1	$ 5.11	$ 5.11
Fuel-Testers	http://www.fuel-testers.com/quikcheck.ht	-	-	1	$ 14.95	$ 14.95
USS2-SV00006	3/8" Electric Solenoid Valve 12-VDC	Amazon	-	1	$ 26.55	$ 26.55
5346K24	1/4" hose 3/8" NPT Barbed Fitting	McMaster Carr	-	1	$ 10.07	$ 10.07
					Overall Cost	**$560.63**

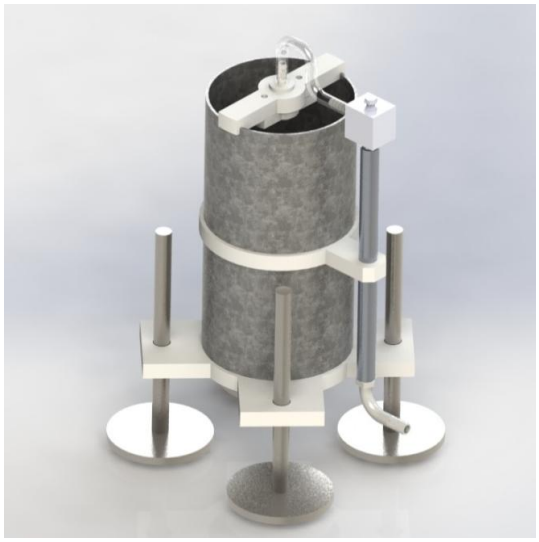

Figure 34: Initial chamber design

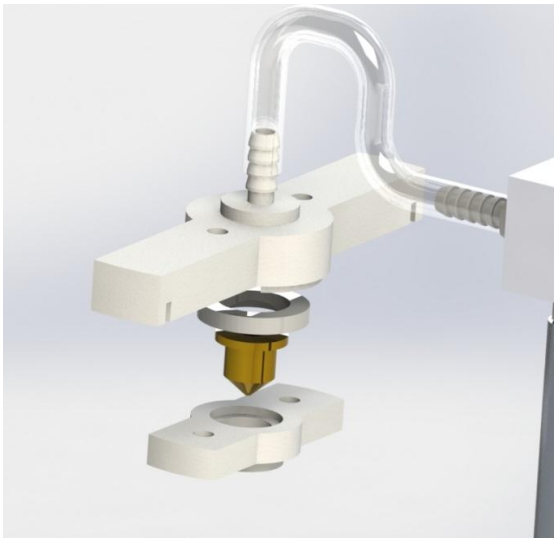

Figure 35: Initial chamber nozzle assembly

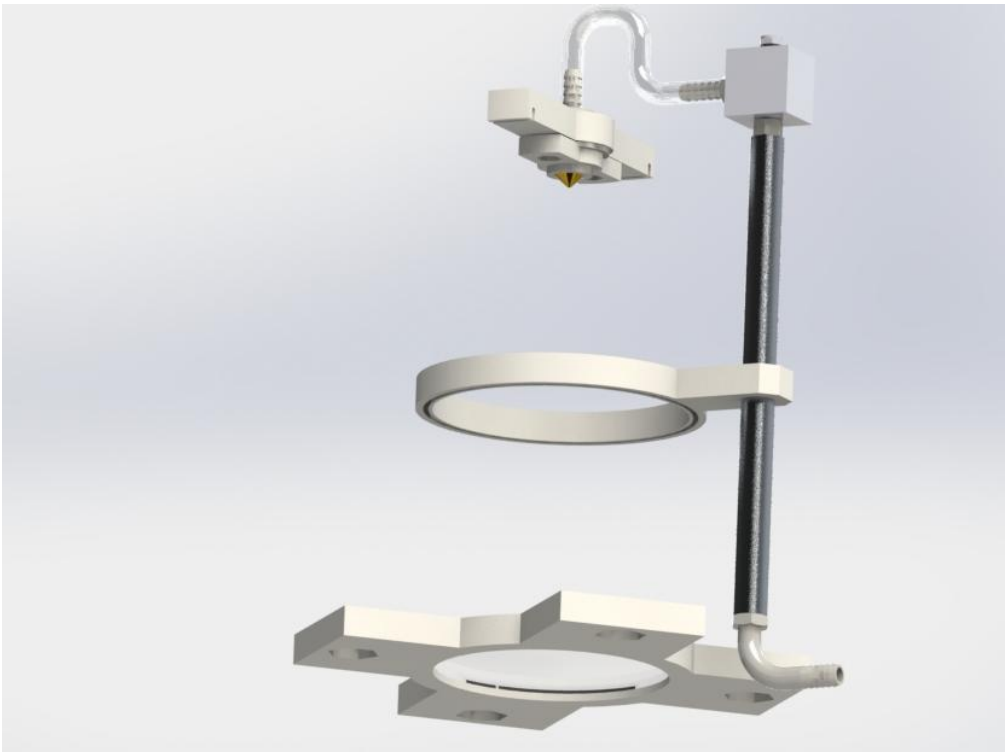

Figure 36: Base, middle, and top of spray chamber and injection unit

APPENDIX C: RAW CHARGING DATA USING TEFLON AND NYLON

Table 5: Raw charging data

Injection #	Gasoline Grade	Injection Pressure [PSI]	Charging Material [Teflon - 3']	Charge [μC]	Charge Density [nC/g]	Charging Material [Nylon - 3']	Charge [μC]	Charge Density [nC/g]
1	87	15	Teflon	-0.00267	**-0.252**	Nylon	-0.00238	**-0.224**
2	87	15	Teflon	-0.00265	**-0.250**	Nylon	-0.00245	**-0.231**
3	87	15	Teflon	-0.00262	**-0.247**	Nylon	-0.00235	**-0.221**
4	87	15	Teflon	-0.00271	**-0.255**	Nylon	-0.00254	**-0.239**
5	87	15	Teflon	-0.00260	**-0.245**	Nylon	-0.00250	**-0.236**
6	87	15	Teflon	-0.00266	**-0.251**	Nylon	-0.00250	**-0.236**
7	87	15	Teflon	-0.00261	**-0.246**	Nylon	-0.00262	**-0.247**
8	87	15	Teflon	-0.00261	**-0.246**	Nylon	-0.00254	**-0.239**
9	87	15	Teflon	-0.00276	**-0.260**	Nylon	-0.00262	**-0.247**
10	87	15	Teflon	-0.00239	**-0.225**	Nylon	-0.00253	**-0.238**
Averages				-0.00263	**-0.248**		-0.00250	**-0.236**
Injection #	**Gasoline Grade**	**Injection Pressure [PSI]**	**Charging Material [Teflon - 3']**	**Charge [μC]**	**Charge Density [nC/g]**	**Charging Material [Nylon - 3']**	**Charge [μC]**	**Charge Density [nC/g]**
1	87	20	Teflon	-0.00324	**-0.264**	Nylon	-0.00272	**-0.222**
2	87	20	Teflon	-0.00325	**-0.265**	Nylon	-0.00285	**-0.232**
3	87	20	Teflon	-0.00324	**-0.264**	Nylon	-0.00278	**-0.227**
4	87	20	Teflon	-0.00315	**-0.257**	Nylon	-0.00255	**-0.208**
5	87	20	Teflon	-0.00326	**-0.266**	Nylon	-0.00276	**-0.225**
6	87	20	Teflon	-0.00301	**-0.245**	Nylon	-0.00269	**-0.219**
7	87	20	Teflon	-0.00322	**-0.263**	Nylon	-0.00284	**-0.232**
8	87	20	Teflon	-0.00320	**-0.261**	Nylon	-0.00258	**-0.210**
9	87	20	Teflon	-0.00319	**-0.260**	Nylon	-0.00287	**-0.234**
10	87	20	Teflon	-0.00300	**-0.245**	Nylon	-0.00294	**-0.240**
Averages				-0.00318	**-0.259**		-0.00276	**-0.225**
Injection #	**Gasoline Grade**	**Injection Pressure [PSI]**	**Charging Material [Teflon - 3']**	**Charge [μC]**	**Charge Density [nC/g]**	**Charging Material [Nylon - 3']**	**Charge [μC]**	**Charge Density [nC/g]**
1	87	25	Teflon	-0.00304	**-0.222**	Nylon	-0.00282	**-0.206**
2	87	25	Teflon	-0.00297	**-0.217**	Nylon	-0.00266	**-0.195**
3	87	25	Teflon	-0.00290	**-0.212**	Nylon	-0.00279	**-0.204**
4	87	25	Teflon	-0.00302	**-0.221**	Nylon	-0.00240	**-0.176**
5	87	25	Teflon	-0.00305	**-0.223**	Nylon	-0.00242	**-0.177**
6	87	25	Teflon	-0.00275	**-0.201**	Nylon	-0.00248	**-0.181**
7	87	25	Teflon	-0.00302	**-0.221**	Nylon	-0.00233	**-0.171**
8	87	25	Teflon	-0.00277	**-0.203**	Nylon	-0.00235	**-0.172**
9	87	25	Teflon	-0.00314	**-0.230**	Nylon	-0.00234	**-0.171**
10	87	25	Teflon	-0.00322	**-0.236**	Nylon	-0.00270	**-0.198**
Averages				-0.00299	**-0.219**		-0.00253	**-0.185**
Injection #	**Gasoline Grade**	**Injection Pressure [PSI]**	**Charging Material [Teflon - 3']**	**Charge [μC]**	**Charge Density [nC/g]**	**Charging Material [Nylon - 3']**	**Charge [μC]**	**Charge Density [nC/g]**
1	87	30	Teflon	-0.00270	**-0.186**	Nylon	-0.00294	**-0.203**
2	87	30	Teflon	-0.00248	**-0.171**	Nylon	-0.00249	**-0.172**
3	87	30	Teflon	-0.00264	**-0.182**	Nylon	-0.00260	**-0.180**
4	87	30	Teflon	-0.00201	**-0.139**	Nylon	-0.00208	**-0.144**
5	87	30	Teflon	-0.00220	**-0.152**	Nylon	-0.00200	**-0.138**
6	87	30	Teflon	-0.00204	**-0.141**	Nylon	-0.00224	**-0.155**
7	87	30	Teflon	-0.00241	**-0.166**	Nylon	-0.00240	**-0.166**
8	87	30	Teflon	-0.00225	**-0.155**	Nylon	-0.00278	**-0.192**
9	87	30	Teflon	-0.00210	**-0.145**	Nylon	-0.00212	**-0.146**
10	87	30	Teflon	-0.00260	**-0.180**	Nylon	-0.00219	**-0.151**
Averages				-0.00234	**-0.162**		-0.00238	**-0.165**

APPENDIX D: RAW DATA OF WEIGHT MEASUREMENTS FOR AUTOVALVE

Table 6: Weight of injection auto valve (15PSI)

Volume Per Spray 15 PSI [1mm3 = 0.001mL]					
Injection #	Density of Fuel [Kg/m^3]	Weight [g]	Weight [kg]	Volume [m^3]	Volume [mm^3]
1	750	10.69	1.069E-02	1.425E-05	14253.3
2	750	10.72	1.072E-02	1.429E-05	14293.3
3	750	10.59	1.059E-02	1.412E-05	14120.0
4	750	10.57	1.057E-02	1.409E-05	14093.3
5	750	10.60	1.060E-02	1.413E-05	14133.3
6	750	10.35	1.035E-02	1.380E-05	13800.0
7	750	10.47	1.047E-02	1.396E-05	13960.0
8	750	10.78	1.078E-02	1.437E-05	14373.3
9	750	10.64	1.064E-02	1.419E-05	14186.7
10	750	10.69	1.069E-02	1.425E-05	14253.3
Average		**10.61**	**1.061E-02**	**1.415E-05**	**14147**

Table 7: Weight of injection auto valve (20PSI)

Volume Per Spray 20 PSI [1mm3 = 0.001mL]					
Injection #	Density of Fuel [Kg/m^3]	Weight [g]	Weight [kg]	Volume [m^3]	Volume [mm^3]
1	750	12.70	1.270E-02	1.693E-05	16933.3
2	750	12.39	1.239E-02	1.652E-05	16520.0
3	750	12.59	1.259E-02	1.679E-05	16786.7
4	750	12.20	1.220E-02	1.627E-05	16266.7
5	750	12.22	1.222E-02	1.629E-05	16293.3
6	750	12.22	1.222E-02	1.629E-05	16293.3
7	750	12.27	1.227E-02	1.636E-05	16360.0
8	750	12.13	1.213E-02	1.617E-05	16173.3
9	750	11.96	1.196E-02	1.595E-05	15946.7
10	750	11.94	1.194E-02	1.592E-05	15920.0
Average		**12.26**	**1.226E-02**	**1.635E-05**	**16349**

Table 8: Weight of injection auto valve (25PSI)

Volume Per Spray 25 PSI [1mm3 = 0.001mL]					
Injection #	Density of Fuel [Kg/m^3]	Weight [g]	Weight [kg]	Volume [m^3]	Volume [mm^3]
1	750	14.25	1.425E-02	1.900E-05	19000.0
2	750	13.78	1.378E-02	1.837E-05	18373.3
3	750	13.48	1.348E-02	1.797E-05	17973.3
4	750	13.75	1.375E-02	1.833E-05	18333.3
5	750	13.80	1.380E-02	1.840E-05	18400.0
6	750	13.53	1.353E-02	1.804E-05	18040.0
7	750	13.51	1.351E-02	1.801E-05	18013.3
8	750	13.34	1.334E-02	1.779E-05	17786.7
9	750	13.56	1.356E-02	1.808E-05	18080.0
10	750	13.64	1.364E-02	1.819E-05	18186.7
Average		**13.66**	**1.366E-02**	**1.822E-05**	**18219**

Table 9: Weight of injection auto valve (30PSI)

Volume Per Spray 30 PSI [1mm3 = 0.001mL]					
Injection #	Density of Fuel [Kg/m^3]	Weight [g]	Weight [kg]	Volume [m^3]	Volume [mm^3]
1	750	14.08	1.408E-02	1.877E-05	18773.3
2	750	13.51	1.351E-02	1.801E-05	18013.3
3	750	14.86	1.486E-02	1.981E-05	19813.3
4	750	14.65	1.465E-02	1.953E-05	19533.3
5	750	14.91	1.491E-02	1.988E-05	19880.0
6	750	14.61	1.461E-02	1.948E-05	19480.0
7	750	13.93	1.393E-02	1.857E-05	18573.3
8	750	14.67	1.467E-02	1.956E-05	19560.0
9	750	14.60	1.460E-02	1.947E-05	19466.7
10	750	14.96	1.496E-02	1.995E-05	19946.7
Average		**14.48**	**1.448E-02**	**1.930E-05**	**19304**

APPENDIX E: RAW DATA WEIGHT MEASUREMENTS FOR PUSH BUTTON VALVE

Table 10: Weight of injection push button valve (15PSI)

Volume Per Spray 15 PSI [1mm3 = 0.001mL]					
Injection #	Density of Fuel [Kg/m^3]	Weight [g]	Weight [kg]	Volume [m^3]	Volume [mm^3]
1	750	9.74	9.740E-03	1.299E-05	12986.7
2	750	10.88	1.088E-02	1.451E-05	14506.7
3	750	9.15	9.150E-03	1.220E-05	12200.0
4	750	10.25	1.025E-02	1.367E-05	13666.7
5	750	11.49	1.149E-02	1.532E-05	15320.0
6	750	11.60	1.160E-02	1.547E-05	15466.7
7	750	11.25	1.125E-02	1.500E-05	15000.0
8	750	10.88	1.088E-02	1.451E-05	14506.7
9	750	10.71	1.071E-02	1.428E-05	14280.0
10	750	11.31	1.131E-02	1.508E-05	15080.0
Average		**10.73**	**1.073E-02**	**1.430E-05**	**14301**

Table 11: Weight of injection push button valve (20PSI)

Volume Per Spray 20 PSI [1mm3 = 0.001mL]					
Injection #	Density of Fuel [Kg/m^3]	Weight [g]	Weight [kg]	Volume [m^3]	Volume [mm^3]
1	750	11.66	1.166E-02	1.555E-05	15546.7
2	750	11.21	1.121E-02	1.495E-05	14946.7
3	750	11.64	1.164E-02	1.552E-05	15520.0
4	750	11.84	1.184E-02	1.579E-05	15786.7
5	750	12.13	1.213E-02	1.617E-05	16173.3
6	750	10.85	1.085E-02	1.447E-05	14466.7
7	750	11.30	1.130E-02	1.507E-05	15066.7
8	750	11.99	1.199E-02	1.599E-05	15986.7
9	750	12.27	1.227E-02	1.636E-05	16360.0
10	750	11.51	1.151E-02	1.535E-05	15346.7
Average		**11.64**	**1.164E-02**	**1.552E-05**	**15520**

Table 12: Weight of injection push button valve (25PSI)

Volume Per Spray 25 PSI [1mm3 = 0.001mL]					
Injection #	Density of Fuel [Kg/m^3]	Weight [g]	Weight [kg]	Volume [m^3]	Volume [mm^3]
1	750	12.38	1.238E-02	1.651E-05	16506.7
2	750	12.54	1.254E-02	1.672E-05	16720.0
3	750	13.28	1.328E-02	1.771E-05	17706.7
4	750	12.00	1.200E-02	1.600E-05	16000.0
5	750	12.81	1.281E-02	1.708E-05	17080.0
6	750	12.45	1.245E-02	1.660E-05	16600.0
7	750	14.21	1.421E-02	1.895E-05	18946.7
8	750	14.05	1.405E-02	1.873E-05	18733.3
9	750	13.02	1.302E-02	1.736E-05	17360.0
10	750	12.02	1.202E-02	1.603E-05	16026.7
Average		**12.88**	**1.288E-02**	**1.717E-05**	**17168**

Table 13: Weight of injection push button valve (30PSI)

Volume Per Spray 30 PSI [1mm3 = 0.001mL]					
Injection #	Density of Fuel [Kg/m^3]	Weight [g]	Weight [kg]	Volume [m^3]	Volume [mm^3]
1	750	12.95	1.295E-02	1.727E-05	17266.7
2	750	14.46	1.446E-02	1.928E-05	19280.0
3	750	11.74	1.174E-02	1.565E-05	15653.3
4	750	12.32	1.232E-02	1.643E-05	16426.7
5	750	13.69	1.369E-02	1.825E-05	18253.3
6	750	12.70	1.270E-02	1.693E-05	16933.3
7	750	15.81	1.581E-02	2.108E-05	21080.0
8	750	12.50	1.250E-02	1.667E-05	16666.7
9	750	13.91	1.391E-02	1.855E-05	18546.7
10	750	12.49	1.249E-02	1.665E-05	16653.3
Average		**13.26**	**1.326E-02**	**1.768E-05**	**17676**

APPENDIX F: RAW DATA OF FRAME DEFINITION FOR MEASUREMENTS

Table 14: Frame definition

Injection	Test Definition	Frame Number Start	Frame Number Stop	Number of Frames	Event Duration at 3000FPS [s]	Top Section Event Duration [s]	Height of Chamber [in]	Velocity [ft/s]	1/8 of Top	1/4 of Top	3/8 of top	1/2 of top	5/8 of Top	3/4 of top	7/8 of top	Last Frame Number of Top Half
1	Electric Field Not Applied (0KV)	2314	2376	62	0.062	0.031	9.1	12.3	2318	2322	2326	2330	2333	2337	2341	2345
2	Electric Field Applied (10 KV)	2646	2699	53	0.053	0.027	9.1	14.4	2649	2653	2656	2659	2663	2666	2669	2673
3	Electric Field Not Applied (0KV)	2178	2229	51	0.051	0.026	9.1	14.9	2181	2184	2188	2191	2194	2197	2200	2204
4	Electric Field Applied (10KV)	2299	2348	49	0.049	0.025	9.1	15.6	2302	2305	2308	2311	2314	2317	2320	2324

APPENDIX G: RAW DATA FOR INJECTION PROFILE MEASUREMENTS OF INJECTION 1-4

Table 15: Measurements of injection 1 (No Electric Field)

Injection Pressure (+/- 2 PSI)	Temperature (°F)	Measurement Depth From Nossel (mm)	X Measurement (mm)	Y Measurement (mm)
20	75	14.5	5.5	6.5
20	75	29.0	6.1	6.1
20	75	43.6	6.1	7.0
20	75	58.1	5.4	8.6
20	75	72.6	4.6	10.4
20	75	87.1	10.9	12.6
20	75	101.6	18.0	18.6
20	75	116.2	24.6	26.5

Table 16: Measurements of injection 2 (Electric Field Applied)

Injection Pressure (+/- 2 PSI)	Temperature (°F)	Measurement Depth From Nozzle (mm)	X Measurement (mm)	Y Measurement (mm)
20	75	14.5	5.1	5.1
20	75	29.0	4.4	6.5
20	75	43.6	3.9	7.3
20	75	58.1	3.7	8.6
20	75	72.6	5.9	10.2
20	75	87.1	10.6	12.7
20	75	101.6	14.4	17.0
20	75	116.2	21.1	20.4

Table 17: Measurements of injection 3 (No Electric Field)

Injection Pressure (+/- 2 PSI)	Temperature (°F)	Measurement Depth From Nozzle (mm)	X Measurement (mm)	Y Measurement (mm)
20	75	14.5	7.7	8.6
20	75	29.0	7.9	10.1
20	75	43.6	5.9	11.1
20	75	58.1	5.5	12.6
20	75	72.6	6.4	13.8
20	75	87.1	11.7	14.4
20	75	101.6	17.7	20.3
20	75	116.2	24.7	26.8

Table 18: Measurements of injection 4 (Electric Field Applied)

Injection Pressure (+/- 2 PSI)	Temperature (°F)	Measurement Depth From Nozzle (mm)	X Measurement (mm)	Y Measurement (mm)
20	75	14.5	5.5	6.5
20	75	29.0	6.1	6.1
20	75	43.6	6.1	7.0
20	75	58.1	5.4	8.6
20	75	72.6	4.6	10.4
20	75	87.1	10.9	12.6
20	75	101.6	18.0	18.6
20	75	116.2	24.6	26.5

APPENDIX H: COMPARISON OF INJECTION PROFILE RECONSTRUCTION USING SOLIDWORKS MODELING

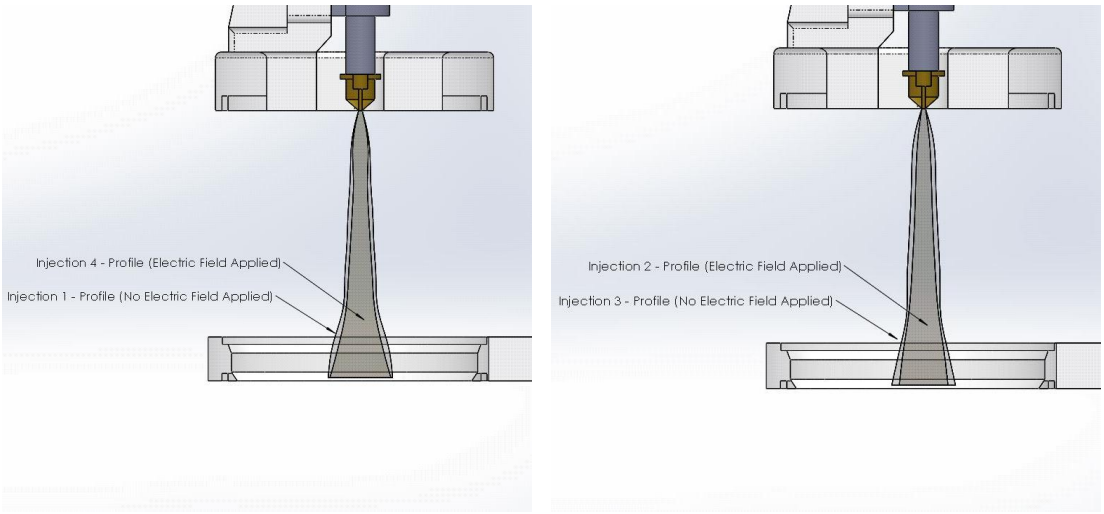

Figure 37: Injection comparison (1 to 4) & (2 to 3)

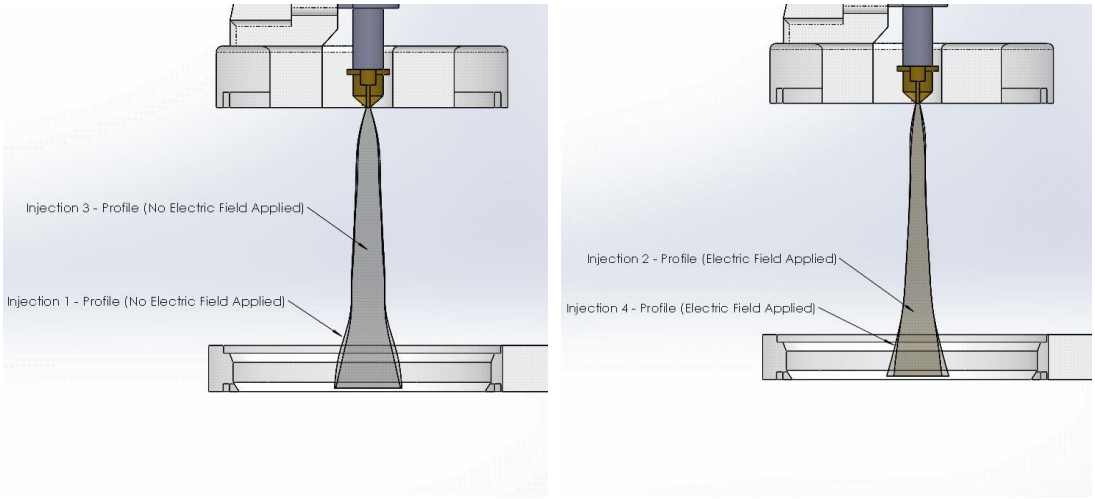

Figure 38: Injection comparison (1 to 3) & (2 To 4)

APPENDIX I: COMSOL UNIFORM DROPLETE DIAMTER MODEL

Table 19: COMSOL definition of parameters test case 1

Name	Expression	Value	Description
D	10.993[cm]	0.10993 m	cylinder diameter
H	10.795[cm]	0.10795 m	cylinder height
dp	5e-5[m]	5E−5 m	droplet diameter
eta_gas	0.0258[N/m]	0.0258 N/m	surface tension of gasoline
eps_0	8.85e-12[F/m]	8.85E−12 F/m	dielectric permittivity of air
qp	8*pi*sqrt(eps_0*eta_gas *(dp/2)^3)	1.5012E−12 C	charge on a droplet (Rayleigh limit)
q_electron	1.6e-19[C]	1.6E−19 C	charge of an electron
gas_density	750[kg/m^3]	750 kg/m³	density of gasoline
dyn_viscosity_air	18.47e-6[Pa*s]	1.847E−5 Pa·s	dynamic viscosity of air
T_cyl	295[K]	295 K	temperature in cylinder
p_cyl	101325[Pa]	1.0133E5 Pa	pressure in cylinder
p_speed	20[m/s]	20 m/s	initial droplet velocity
p_number	50	50	number of released droplets
V_el	0[V]	0 V	potential applied to cylinder
t_lim	27[ms]	0.027 s	length of the injection process
q_droplet	-1.5217e-13[C]	−1.5217E−13 C	Charge of the Droplet

Table 20: COMSOL definition of test parameters test case 2

Name	Expression	Value	Description
D	10.993[cm]	0.10993 m	cylinder diameter
H	10.795[cm]	0.10795 m	cylinder height
dp	5e-5[m]	5E−5 m	droplet diameter
eta_gas	0.0258[N/m]	0.0258 N/m	surface tension of gasoline
eps_0	8.85e-12[F/m]	8.85E−12 F/m	dielectric permittivity of air
qp	8*pi*sqrt(eps_0*eta_gas *(dp/2)^3)	1.5012E−12 C	charge on a droplet (Rayleigh limit)
q_electron	1.6e-19[C]	1.6E−19 C	charge of an electron
gas_density	750[kg/m^3]	750 kg/m³	density of gasoline
dyn_viscosity_air	18.47e-6[Pa*s]	1.847E−5 Pa·s	dynamic viscosity of air
T_cyl	295[K]	295 K	temperature in cylinder
p_cyl	101325[Pa]	1.0133E5 Pa	pressure in cylinder
p_speed	20[m/s]	20 m/s	initial droplet velocity
p_number	50	50	number of released droplets
V_el	-10000[V]	−10000 V	potential applied to cylinder
t_lim	27[ms]	0.027 s	length of the injection process
q_droplet	-1.5217e-13[C]	−1.5217E−13 C	Charge of the Droplet